STEPS TOWARD DETERMINATION OF THE SIZE AND STRUCTURE OF THE BROAD-LINE REGION IN ACTIVE GALACTIC NUCLEI. I. AN 8 MONTH CAMPAIGN OF MONITORING NGC 5548 WITH *IUE*

J. CLAVEL,[1] G. A. REICHERT,[2] D. ALLOIN,[3] D. M. CRENSHAW,[2] G. KRISS,[4] J. H. KROLIK,[4] M. A. MALKAN,[5] H. NETZER,[6]
B. M. PETERSON,[7] W. WAMSTEKER,[1] A. ALTAMORE,[8] T. BARIBAUD,[3] P. BARR,[9] S. BECK,[6] L. BINETTE,[10] G. E. BROMAGE,[11]
N. BROSCH,[6] A. I. DIAZ,[12] A. V. FILIPPENKO,[13] K. FRICKE,[14] C. M. GASKELL,[15] P. GIOMMI,[9] I. S. GLASS,[16]
P. GONDHALEKAR,[11] R. L. HACKNEY,[17] J. P. HALPERN,[18] D. J. HUTTER,[2] S. JÖRSÄTER,[19] A. L. KINNEY,[20]
W. KOLLATSCHNY,[14] A. KORATKAR,[15] K. T. KORISTA,[7] A. LAOR,[6] J. P. LASOTA,[3] E. LEIBOWITZ,[6]
D. MAOZ,[6] P. G. MARTIN,[10] T. MAZEH,[6] E. J. A. MEURS,[21] A. D. NAIR,[22] P. O'BRIEN,[23]
D. PELAT,[3] E. PEREZ,[24] G. C. PEROLA,[8] R. L. PTAK,[22] P. RODRIGUEZ-PASCUAL,[25]
E. I. ROSENBLATT,[26] A. C. SADUN,[27] M. SANTOS-LLEO,[25] R. A. SHAW,[2]
P. S. SMITH,[28] G. M. STIRPE,[29] R. STONER,[22] W. H. SUN,[30]
M.-H. ULRICH,[31] E. VAN GRONINGEN,[32] AND W. ZHENG[33]

ABSTRACT

We present emission-line and ultraviolet continuum observations of a type I Seyfert galaxy in which the time resolution is adequate for describing the character of variability. Using the *IUE* satellite, the nucleus of NGC 5548 was observed every 4 days for a period of 8 months. Its mean properties—continuum shape, line ratios—are not unusual for type I Seyfert galaxies, but it was found to be strongly variable. The ultraviolet continuum flux and broad emission line fluxes varied significantly, going through three large maxima and three deep minima. The ratio of maximum to minimum flux was $\simeq 4.5$ for the continuum at 1350 Å, and the continuum was significantly bluer when it was brighter. The high-ionization emission lines showed the strongest variations, with N v $\lambda 1240$ and He II $\lambda 1640$ exhibiting maximum-to-minimum flux ratios as high as those of the continuum. Intermediate-ionization lines, including Lyα $\lambda 1216$, C IV $\lambda 1549$, and C III] $\lambda 1909$, had maximum-to-minimum amplitudes of ~ 2, and Mg II $\lambda 2798$, the lowest ionization line, exhibited the smallest amplitude fluctuations, ~ 1.3. The great majority of all variations were well resolved in time. Apart from Mg II $\lambda 2798$, the emission-line variations correlate extremely well with those of the 1350 Å continuum if allowance is made for a systematic delay, lending qualitative support to the view that photoionization by the nuclear con-

[1] ESA *IUE* Observatory, P.O. Box 50727, 28080 Madrid, Spain.
[2] Astronomy Program, Computer Sciences Corporation, Goddard Space Flight Center, Code 684.9, Building 21, Greenbelt, MD 20771.
[3] Observatoire de Paris, 92195 Meudon Principal Cedex, France.
[4] The Johns Hopkins University, Department of Physics and Astronomy, Baltimore, MD 21218.
[5] University of California, Department of Astronomy, Los Angeles, CA 90024-1562.
[6] School of Physics and Astronomy and Wise Observatory, Tel-Aviv University, Tel Aviv 69978, Israel.
[7] Department of Astronomy, Ohio State University, 174 West 18th Avenue, Columbus, OH 43210.
[8] Istituto Astronomico dell'Università, Via Lancisi 29, I-00161 Rome, Italy.
[9] *EXOSAT* Observatory, Astrophysics Division of ESA, ESTEC, Postbus 299, 2200-AG Noordwijk, The Netherlands.
[10] CITA, McLennan Laboratories, University of Toronto, 60 St. George Street, Toronto, Ontario, Canada M5S 1A1.
[11] Astrophysics Group, Rutherford Appleton Laboratory, Chilton, Didcot, Oxfordshire OX11 0QX, United Kingdom.
[12] Departamento de Física Teórica, C-XI, Universidad Autónoma, Cantoblanco, 28049 - Madrid, Spain.
[13] Department of Astronomy, University of California at Berkeley, Berkeley, CA 94720.
[14] Universitätssternwarte, Geismarlandstrasse 11, D-3400 Göttingen, Germany.
[15] University of Michigan, Astronomy Department, Dennison Building, Ann Arbor, MI 48109-1090.
[16] South African Astronomical Observatory, P.O. Box 9, Observatory, 7935 South Africa.
[17] Western Kentucky University, Department of Physics and Astronomy, Bowling Green, KY 42101.
[18] Columbia University, Department of Physics, 538 West 120th Street, New York, NY 10027.
[19] ESA STECF, Karl-Schwarzschild-Strasse 2, D-8046 Garching-bei-München, Germany.
[20] Space Telescope Science Institute, 3700 San Martin Drive, Baltimore, MD 21218.
[21] Max-Planck-Institut für Extraterrestrische Physik, Giessenbachstrasse, D-80416 Garching-bei-München, Germany.
[22] Bowling Green State University, Physics and Astronomy Department, Bowling Green, OH 43403.
[23] Department of Astronomy, University College London, Gower Street, London WC1E 6BT, United Kingdom.
[24] Instituto de Astrofísica de Canarias, 38200 La Laguna, Tenerife, Spain.
[25] Instituto de Astronomia, Universidad Complutense, 28040 Madrid 3, Spain.
[26] University of California at San Diego, CASS, Code C-011, La Jolla, CA 92093.
[27] Bradley Observatory, Agnes Scott College, Decatur, GA 30030.
[28] Steward Observatory, University of Arizona, Tucson, AZ 85721.
[29] Osservatorio Astronomico di Bologna, Via Zamboni 33, I-40126 Bologna, Italy.
[30] Laboratory for Astronomy and Solar Physics, NASA/GSFC, Greenbelt, MD 20771.
[31] European Southern Observatory, Karl-Schwarzschild-Strasse 2, D-8046 Garching-bei-München, Germany.
[32] Uppsala Astronomical Observatory, Box 515, S-75120 Uppsala, Sweden.
[33] University of Alabama, Department of Physics and Astronomy, Tuscaloosa, AL 35487-0324.

tinuum is responsible for driving the emission lines. The delay of a given line seems to depend on the degree of ionization of its species. The He II λ1640 and N V λ1240 features exhibit the shortest delay, $\Delta t \sim$ 4–10 days, while the Lyα λ1216 and C IV λ1549 lines yield 8–16 days. The Si IV + O IV] λ1402 feature and the C III] λ1909 line exhibit significantly larger delays, between 12 and 34 days. In the case of Mg II λ2798, the cross-correlation is broad and shallow, so that the delay is only loosely constrained, $\Delta t \sim$ 34–72 days.

Subject headings: galaxies: individual (NGC 5548) — galaxies: nuclei — galaxies: Seyfert — ultraviolet: spectra

I. INTRODUCTION

For more than 20 years it has been known that the fluxes of the continuum and broad emission lines of active galactic nuclei (AGNs) are variable (Andrillat and Souffrin 1968; Dibai and Pronik 1967; Fitch, Pacholczyk, and Weymann 1967). It was also realized quite early that the broad emission line and continuum variations are closely related (Cherepashchuk and Lyutyi 1973), as would be expected if the gas responsible for these lines is photoionized and heated by the continuum source. If photoionization is indeed the correct explanation for the emission lines' source of energy, the local response to changes in the continuum flux takes less than 1 hr, but the line-emitting region is predicted to be much larger—light-days to many light-years across—scaling crudely as $L^{1/2}$, where L is the ionizing luminosity of the nucleus (Davidson and Netzer 1979). Therefore, one would expect emission-line fluctuations to follow continuum fluctuations, but spread out and delayed by an amount comparable to the light-travel time across the emission-line region.

In principle, it is possible to deconvolve the emission-line and continuum light curves to infer the detailed structure of the emission-line region (Blandford and McKee 1982; Capriotti, Foltz, and Peterson 1982). It might be possible to obtain by this method the geometrical configuration and the run of physical conditions of the broad-line region (BLR) gas as a function of distance from the central source. Such a deconvolution would amount to a direct test of the size prediction made by photoionization models. Not surprisingly, therefore, much observational effort has been recently devoted to the spectrophotometric monitoring of active galaxies (see, e.g., the review by Peterson 1988a and references therein). The best-studied sources so far are, in order of decreasing luminosity, Fairall 9 (Clavel, Wamsteker, and Glass 1989; Koratkar and Gaskell 1989), Akn 120 (Peterson, Korista, and Wagner 1989), Mrk 279 (Maoz *et al.* 1990), NGC 5548 (Netzer *et al.* 1990; Wamsteker *et al.* 1990; Peterson *et al.* 1990b; Rosenblatt and Malkan 1990), NGC 4151 (Ulrich *et al.* 1984; Gaskell and Sparke 1986; Clavel *et al.* 1987). However, all of these studies have suffered from at least one of the following problems: inadequate temporal resolution, insufficient span of observations, too many gaps in the time series, or low ratio of fluctuation amplitude to measurement uncertainty. In the case of the optical studies, the interpretation is also hampered by the considerable difference in photon energy between the continuum band monitored (frequently the *B*-band) and the continuum band which actually drives the lines (13 eV to $\sim$5 keV, depending on the individual line).

We therefore initiated a program whose object was to circumvent all these problems. The choice of the target (NGC 5548) was mainly driven by practical considerations. A large apparent brightness, a long *IUE* observability window (8 months), and a documented history of strong line and continuum variability (e.g., Gregory, Ptak, and Stoner 1982; Barr, Willis, and Wilson 1983; Peterson *et al.* 1990b; Wamsteker *et*

al. 1990) were the main selection criteria. Regular observations are essential to obtain a good description of the power spectrum of fluctuations, and are an absolute prerequisite to carrying out the deconvolution program outlined by Blandford and McKee (1982). The sampling interval of 4 days was determined by examination of previous observations and by comparison with a rough estimate from photoionization modeling of the light-travel time across the broad emission line region. We chose to observe in the ultraviolet to solve other problems. The observed continuum is closer in wavelength to the ionizing continuum driving the strong emission lines, and there is little dilution of the observed continuum by stellar light. The UV emission lines dominate the cooling of the broad-line clouds, and they span a wide range of ionization states. Moreover, by observing from space we were able to achieve greater photometric accuracy and eliminate interruptions to the observing schedule posed by weather or lunar phase. However, in order to maximize the scientific return from this effort, a parallel ground-based monitoring program was initiated (Peterson 1988b). Its results will be reported separately (Peterson *et al.* 1990a).

NGC 5548 is a low-redshift ($z = 0.0174$) Seyfert I galaxy. In the radio band, it shows a weak compact nuclear source straddled by two lobes with a total extent of 4.4 kpc (Wilson and Ulvestad 1982). Deep [O III] λ5007 exposures reveal an extended (4.0 kpc $\times$ 2.7 kpc) emission-line region roughly aligned with the radio structure (Wilson *et al.* 1989). NGC 5548 was detected out to 100 μm by the *IRAS* satellite (Edelson and Malkan 1986). In X-rays it qualifies as a low-luminosity AGN, with $L_{2-10\,keV} = 4.5 \times 10^{43}$ ergs s^{-1} (Turner and Pounds 1989; Kaastra and Barr 1989). Branduardi-Raymont (1988) reported a possible correlation between the variations at X-ray, UV, and optical wavelengths. This last author also presented evidence of X-ray spectral variations, the 2–10 keV spectrum becoming systematically softer when the source brightens. These spectral changes may be related to the existence of a "soft X-ray excess" which dominates the emission below 1 keV (Turner and Pounds 1989). A strong correlation between the ultraviolet and the optical variations is indicated by the results of Wamsteker *et al.* (1990), with the continuum becoming slightly bluer when brighter. Netzer *et al.* (1990) found that the variations of the Hα λ6563 and Hβ λ4861 emission lines lag behind those of the blue continuum by 7 $\pm$ 3 days.

II. THE OBSERVATIONS

The nucleus of NGC 5548 was observed at 60 different epochs in the low-resolution mode (1000 km s^{-1}) and through the large apertures (10″ $\times$ 20″) of the *IUE* (Boggess *et al.* 1978a, b; Faelker, Gordon, and Sandford 1987) spectrographs. Each epoch lasted about 4 hr (exceptionally 8 hr), during which one LWP (1900–3300 Å) and at least one SWP (1170–1970 Å) spectrum were obtained. In total, the data base contains 85 SWP spectra and 61 LWP spectra. Their sequential numbers

TABLE 1

LOG OF *IUE* OBSERVATIONS

Image N°	Date U.T.	Start Time (Hour:Min:Sec)	J.D. (-2,440,000)	Duration (Seconds)	FES (Counts)	Notes
LWP14644	14DEC88	14:02:06	7510.08479	3900	53	
SWP35029	14DEC88	15:20:48	7510.13944	5220	47	
SWP35070	18DEC88	13:57:29	7514.08159	5400	53	
LWP14664	18DEC88	15:35:48	7514.14986	3900	53	
SWP35097	22DEC88	10:13:03	7517.92573	5400	52	
LWP14693	22DEC88	11:51:46	7517.99428	3900	54	
SWP35138	26DEC88	14:11:05	7522.09103	5400	51	Cosmic ray
LWP14721	26DEC88	15:48:08	7522.15843	3600	54	
SWP35190	30DEC88	14:22:39	7526.09906	5400	54	
LWP14744	30DEC88	16:01:25	7526.16765	3000	56	
SWP35242	03JAN89	12:18:26	7530.01280	6000	49	
LWP14763	03JAN89	14:05:03	7530.08684	2400	50	
SWP35284	07JAN89	12:03:05	7534.00214	5400	54	
LWP14784	07JAN89	13:43:20	7534.07176	3900	56	
SWP35323	11JAN89	16:04:58	7538.17012	5100	54	
SWP35324	11JAN89	18:22:16	7538.26546	4800	56	
LWP14802	11JAN89	17:43:10	7538.23831	3600	55	
SWP35325	11JAN89	20:30:59	7538.35485	4800	62	
SWP35363	16JAN89	17:08:41	7543.21436	3900	56	
LWP14848	16JAN89	18:21:42	7543.26507	3000	57	
SWP35364	16JAN89	19:20:26	7543.30586	3300	60	
SWP35383	19JAN89	12:12:23	7546.00860	5400	54	
LWP14870	19JAN89	13:52:39	7546.07823	3600	55	
SWP35393	23JAN89	07:55:58	7549.83053	5400	55	
LWP14901	23JAN89	09:33:24	7549.89819	3900	57	
SWP35416	26JAN89	15:50:35	7553.16013	3600	55	
LWP14927	26JAN89	16:58:51	7553.20753	2700	56	
SWP35461	30JAN89	15:49:26	7557.15933	3600	53	
LWP14945	30JAN89	16:58:29	7557.20728	2700	53	
SWP35462	30JAN89	17:50:57	7557.24372	3600	56	
SWP35478	04FEB89	08:31:38	7561.85530	5400	50	
LWP14964	04FEB89	10:09:34	7561.92331	3000	50	
LWP14970	05FEB89	17:58:00	7563.24861	3900	57	Few px sat.
SWP35511	08FEB89	08:54:23	7565.87110	4800	51	Vignetting
LWP14989	08FEB89	10:21:18	7565.93146	2700	51	Vignetting
SWP35538	12FEB89	08:16:35	7569.84485	6000	46	
LWP15024	12FEB89	10:03:38	7569.91919	3600	48	
SWP35569	16FEB89	05:06:58	7573.71317	5400	44	
LWP15045	16FEB89	06:57:33	7573.78997	2100	45	
LWP15067	20FEB89	09:06:09	7577.87927	3000	44	
SWP35595	20FEB89	10:03:43	7577.91925	3240	44	
SWP35617	24FEB89	08:46:33	7581.86566	5400	44	
LWP15087	24FEB89	10:26:38	7581.93516	2100	45	
LWP15113	28FEB89	11:45:55	7585.99022	3000	44	
SWP35636	28FEB89	12:19:21	7586.01344	5400	46	
SWP35637	28FEB89	14:34:09	7586.10705	1620	47	
SWP35676	04MAR89	11:46:48	7589.99083	4800	47	
LWP15131	04MAR89	13:15:21	7590.05233	2700	48	
SWP35677	04MAR89	14:08:11	7590.08902	2700	49	
SWP35712	08MAR89	12:00:48	7594.00056	4800	46	
LWP15152	08MAR89	13:30:03	7594.06253	2700	49	

are listed in the observing log of Table 1. The acquisition procedure was standard. Particular care was taken to center accurately the nucleus inside the aperture with the Fine Error Sensor (FES) star tracker. The exposure times were chosen such that the maximum allowable signal level is reached at the top of the Lyα λ1216 and Mg II λ2798 emission lines. Three

LWP spectra and one SWP spectrum turned out to have 1 pixel saturated each. Such a level of saturation is so small that it has no significant impact. A few hours prior to the observations of 1989 February 8, the spectrograph apertures had been closed. Closing the aperture has the effect of shifting the FES reference frame by up to 5″ (Sonneborn *et al.* 1987). The posi-

TABLE 1—Continued

Image N°	Date U.T.	Start Time (Hour:Min:Sec)	J.D. (-2,440,000)	Duration (Seconds)	FES (Counts)	Notes
SWP35713	08MAR89	14:25:47	7594.10124	1800	49	
SWP35753	12MAR89	11:57:05	7597.99797	4200	46	
LWP15174	12MAR89	13:17:11	7598.05360	2700	51	
SWP35754	12MAR89	14:09:39	7598.09003	2400	51	
SWP35789	16MAR89	11:55:51	7601.99712	4200	47	
LWP15202	16MAR89	13:17:10	7602.05359	3000	50	
SWP35790	16MAR89	14:16:10	7602.09456	3300	50	
SWP35823	20MAR89	12:13:43	7606.00953	3900	49	
LWP15227	20MAR89	13:30:00	7606.06250	3000	51	
SWP35824	20MAR89	14:27:57	7606.10274	1440	53	
SWP35849	24MAR89	09:42:53	7609.90478	4200	48	
SWP35880	28MAR89	04:26:21	7613.68497	5400	48	
LWP15254	28MAR89	06:07:30	7613.75521	3600	50	
LWP15281	01APR89	01:33:55	7617.56522	3600	57	
SWP35907	01APR89	02:57:28	7617.62324	6000	49	
SWP35936	05APR89	02:07:17	7621.58839	5400	53	
LWP15305	05APR89	03:45:35	7621.65666	3900	54	
SWP35965	09APR89	02:10:20	7625.59051	5400	53	
LWP15327	09APR89	03:49:46	7625.65956	3900	56	1 px sat.
SWP35996	13APR89	05:45:37	7629.74001	4800	56	
LWP15350	13APR89	07:16:50	7629.80336	3300	54	
SWP35997	13APR89	08:17:12	7629.84528	2100	53	
SWP36018	17APR89	10:13:11	7633.92582	3900	53	
LWP15361	17APR89	11:29:39	7633.97892	3000	55	
SWP36019	17APR89	12:25:02	7634.01738	1560	57	
SWP36055	21APR89	09:59:19	7637.91619	3900	55	
LWP15385	21APR89	11:15:44	7637.96926	3000	55	
SWP36056	21APR89	12:17:01	7638.01182	2040	55	
SWP36089	25APR89	11:32:28	7641.98088	3900	54	
LWP15406	25APR89	12:45:28	7642.03157	3000	54	
SWP36159	29APR89	09:45:13	7645.90640	3600	56	
LWP15410	29APR89	10:56:11	7645.95568	2700	56	
SWP36160	29APR89	11:50:06	7645.99312	3600	56	
SWP36184	03MAY89	08:09:39	7649.84003	3900	52	
LWP15443	03MAY89	09:26:41	7649.89353	3000	55	
SWP36185	03MAY89	10:26:26	7649.93502	1500	54	
SWP36210	07MAY89	08:24:11	7653.85013	3900	54	
LWP15473	07MAY89	09:37:27	7653.90101	3000	55	
SWP36240	11MAY89	00:34:22	7657.52387	4200	57	
LWP15492	11MAY89	01:53:29	7657.57881	3300	56	
SWP36264	15MAY89	00:02:20	7661.50162	4500	53	
LWP15517	15MAY89	01:32:48	7661.56444	3600	51	
SWP36296	18MAY89	23:52:43	7665.49494	4800	52	1 px sat.
LWP15542	19MAY89	01:39:25	7665.56904	3600	53	1 px sat.
SWP36322	23MAY89	00:02:38	7669.50183	3600	61	
LWP15578	23MAY89	01:13:45	7669.55122	3600	51	1 px sat.
SWP36323	23MAY89	02:22:23	7669.59888	3000	49	
LWP15606	27MAY89	00:11:45	7673.50816	3300	50	
SWP36345	27MAY89	01:13:46	7673.55123	4500	50	
SWP36369	31MAY89	00:27:43	7677.51925	4500	50	

tion of the guide star as measured by the FES, as well as the global shift of the wavelength scales on that day, show that the nucleus of NGC 5548 was offset by 4″ from the center of the aperture, along its small axis. The data therefore suffered from significant vignetting.

Immediately before (and some time after) each exposure, the optical brightness of NGC 5548 was recorded with the FES star tracker on board *IUE*. The FES is an image dissector which provides broad-band photometric flux measurements down to an rms accuracy of ±0.07 mag (Holm and Crabb 1979; Barylak, Wasatonic, and Imhoff 1984). The response curve of its S-20 photocathode extends from 3900 to 9000 Å, with a sharp maximum of sensitivity near 4600 Å (Holm and Rice 1981). For an AGN–type spectrum, its effective wavelength is ∼5000 Å. In its "overlap" tracking mode, the equivalent aperture of the FES is 12″ × 12″ squared. Hence, the NGC 5548 count rates include a significant contribution from the underlying stellar population. The FES is known to suffer from

TABLE 1—*Continued*

Image N°	Date U.T.	Start Time (Hour:Min:Sec)	J.D. (-2,440,000)	Duration (Seconds)	FES (Counts)	Notes
LWP15626	31MAY89	01:51:28	7677.57741	3600	48	
SWP36385	03JUN89	05:52:41	7680.74492	4500	51	
LWP15647	03JUN89	07:26:28	7680.81005	3000	50	
SWP36386	03JUN89	08:27:14	7680.85225	1440	50	
LWP15670	07JUN89	09:17:51	7684.88740	3000	49	
SWP36411	07JUN89	10:17:43	7684.92897	4500	49	
LWP15671	07JUN89	11:42:09	7684.98760	2100	50	
SWP36412	07JUN89	12:28:05	7685.01950	1500	49	
SWP36446	11JUN89	05:49:08	7688.74245	4500	47	
LWP15702	11JUN89	07:13:15	7688.80087	3000	47	
SWP36447	11JUN89	08:09:41	7688.84006	2400	47	
SWP36509	15JUN89	05:49:37	7692.74279	4500	47	
LWP15729	15JUN89	07:13:55	7692.80133	3000	48	
SWP36510	15JUN89	08:13:54	7692.84299	2400	46	
SWP36551	19JUN89	06:09:37	7696.75668	4500	48	
LWP15750	19JUN89	07:33:19	7696.81480	3000	48	
SWP36567	23JUN89	05:45:16	7700.73977	4500	46	
LWP15773	23JUN89	07:09:40	7700.79838	3000	47	
SWP36568	23JUN89	08:07:33	7700.83858	2580	48	
SWP36580	27JUN89	22:18:48	7705.42972	4800	49	
LWP15805	27JUN89	23:47:17	7705.49117	3600	48	
SWP36595	01JUL89	20:09:45	7709.34010	4800	48	
LWP15822	01JUL89	21:40:02	7709.40280	3600	50	
SWP36616	05JUL89	20:02:07	7713.33480	4800	49	
LWP15857	05JUL89	21:30:45	7713.39635	3600	50	
SWP36648	09JUL89	19:44:42	7717.32271	4200	53	
LWP15889	09JUL89	21:05:23	7717.37874	3300	53	
SWP36675	13JUL89	20:02:18	7721.33493	4800	49	
LWP15912	13JUL89	21:40:48	7721.40333	3600	49	
SWP36691	17JUL89	20:04:52	7725.33671	4200	44	
LWP15948	17JUL89	21:23:55	7725.39161	3300	48	
SWP36692	17JUL89	22:27:51	7725.43601	1800	45	
SWP36715	22JUL89	04:04:51	7729.67003	4500	46	
LWP15976	22JUL89	05:29:11	7729.72860	3000	48	
SWP36716	22JUL89	06:25:40	7729.76782	1500	49	
SWP36739	26JUL89	04:19:38	7733.68030	4500	45	
LWP15989	26JUL89	05:40:13	7733.73626	3000	46	
SWP36740	26JUL89	06:36:04	7733.77505	1200	46	
SWP36758	30JUL89	03:53:47	7737.66235	4500	45	
LWP16019	30JUL89	05:18:05	7737.72089	3000	45	
SWP36759	30JUL89	06:13:34	7737.75942	2100	45	
SWP36783	03AUG89	01:58:38	7741.58238	5700	43	
LWP16055	03AUG89	03:44:06	7741.65563	3900	41	
SWP36805	07AUG89	01:21:53	7745.55686	5100	43	
LWP16083	07AUG89	02:53:04	7745.62019	2580	44	

a gradual loss of sensitivity (Barylak, Wasatonic, and Imhoff 1984). However, the decrease in efficiency over an 8 month period is so small that it may be neglected. The FES counts are listed in Table 1.

III. DATA REDUCTION AND ANALYSIS

In order to test the robustness of our results, the ultraviolet spectra were reduced independently using two different methods. Similarly, the continuum and line fluxes were independently measured by different people using different procedures. We now describe briefly each of these methods.

a) IUESIPS Data Reduction and Flux Summation

In the first method, the spectra have been reduced with the standard *IUE* Spectral Image Processing System (IUESIPS), which is routinely used by the *IUE* project to process guest observers' data (Turnrose and Thompson 1984; Harris and Sonneborn 1987). After the pixel-to-pixel photometric calibration ("ITF correction"), a "gross" spectrum is extracted by summing at each wavelength step all the flux which falls into an 18 pixel wide (19″.4) slit. A smoothed background measured on each side of the data strip is then subtracted from the gross

spectrum, and the resulting net flux is multiplied by the absolute calibration files and divided by the exposure time. The loss of sensitivity of the SWP and LWP cameras over an 8 month period is so small that corrections are not necessary. No correction for the temperature of the camera head amplifier (THDA) was applied either. While involving uncertainties, this correction would change the flux values by at most a fraction of a percent. Obvious blemishes and cosmic-ray hits have been manually removed from the two-dimensional "extended line-by-line" (ELBL) spectral images (Munoz-Peiro 1985). In image SWP 35138, a cosmic ray centered at $\lambda_{rest} = 1270$ Å was too strong and extended to be removed in a reliable way. All the SWP spectra were aligned so that the peak of the Lyα emission line always falls at 1215.67 Å (rest wavelength). For well-exposed spectra, the relative accuracy ("repeatability") of *IUE* flux measurements in 25 Å bins is 1.5%–2% (Bohlin et al. 1980).

The actual measurement of the line and continuum flux was done as follows. As a first step, all the SWP and all the LWP spectra were averaged together. The high signal-to-noise ratio mean spectra thus obtained were used to select the most representative continuum and line integration intervals. The same intervals were used for all spectra. The measurement process itself was completely impersonal and fully automated. The continuum was measured at three different locations: F_{1350} and F_{1840} represent the mean continuum flux over 40 Å intervals centered at 1350 and 1840 Å, respectively (unless otherwise specified, all wavelengths are expressed in the rest frame of NGC 5548). F_{2670} was measured in a 50 Å bin centered at 2670 Å. We caution here that these continuum measurements unavoidably contain some emission-line flux. The least affected is F_{1350}, since the only potential contaminator, C II $\lambda1335$, is not recognizable in any of the individual or averaged spectra (Fig. 1). F_{1840} is slightly contaminated by weak and blended low-contrast Fe II features as well as by Balmer continuum (Bac) emission from the BLR (Wamsteker et al. 1990). These

features could contribute ≃10% to the flux in this band. The 2670 Å interval sits right on top of the "small bump," but it lies in a local minimum of the Fe II emission models of Wills, Netzer, and Wills (1985). It is difficult to estimate precisely the amount of contamination, as this would require a somewhat model-dependent spectral decomposition of the optical-UV energy distribution of NGC 5548. However, the work of Wamsteker and collaborators indicates that between 30% and 40% of the F_{2670} flux may be due to Fe II + (Bac) emission.

We have measured the flux of the strong H Lyα $\lambda1216$, C IV $\lambda1549$ emission lines as well as that of the weaker Mg II $\lambda2798$, C III] $\lambda1909$, He II $\lambda1640$ and Si IV + O IV] $\lambda1402$ lines. The fluxes were computed by summing all the flux above the continuum in a given interval. The intervals of integration were 1207–1250 Å, 1484–1610 Å, 2752–2845 Å, 1867–1909 Å, 1622–1677 Å, and 1375–1420 Å for the Lyα, C IV, Mg II, C III], He II (+O III]), and Si IV (+O IV]) lines, respectively. The Lyα $\lambda1216$ interval avoids the strong geocoronal Lyα emission line but misses a significant fraction of the blue-wing flux. The choice of the integration interval for C III] was driven by the fact that the IUESIPS SWP calibration does not extend beyond 1950 Å, i.e., 1917 Å in the rest frame of NGC 5548. Assuming that the line profile is symmetrical, the flux measured over the 1867–1909 Å range was multiplied by 2 to account for the missing red wing.

The flux of the local continuum underneath each feature was assumed to be independent of wavelength over the interval of integration (i.e., $F_\lambda = $ constant). For the Lyα $\lambda1216$ and Si IV + O IV] $\lambda1402$ lines, the flux is the mean of F_{1350} and F_{1446}, where F_{1446} is the average flux over the 1425–1466 Å interval. The continuum flux underneath C IV $\lambda1549$ and He II $\lambda1640$ is the mean of F_{1446} and F_{1840}. We have averaged the flux over the 2644–2683 Å and 2883–2959 Å intervals and used the mean of the two to set the continuum level below Mg II $\lambda2798$. Finally, F_{1840} defines the continuum flux underlying the C III] $\lambda1909$ line.

No evidence was found for variability on a time scale of a few hours. Hence, the 25 pairs of SWP spectra obtained on the same day have been used to estimate the repeatability of individual measurements. For each pair of measurements, we computed a mean and a standard deviation. Plots of these deviations against the mean flux or against the shortest of the two exposure times show a scatter diagram. This is because almost all spectra were optimally exposed, with roughly the same number of counts per pixel. There is a weak tendency, however, for the few spectra which had a very short exposure time to yield significantly larger deviations. Hence, we have assigned to each individual measurement an error which is simply the unweighted mean of the 25 standard deviations. For the nine SWP spectra which had an exposure time less than 2000 s, these errors were further multiplied by 1.5.

There exists only one pair of LWP spectra obtained a few hours apart. Hence, a different method had to be used to derive the uncertainties attached to the measurements made in that wavelength range. The error on the Mg II $\lambda2798$ line flux was obtained by scaling the error on Lyα $\lambda1216$ by the square root of the ratio of the mean raw *IUE* data numbers (i.e., counts) in the two lines. The error on the 2670 Å continuum flux is simply the standard deviation of the flux in the 50 Å bin.

FIG. 1.—SWP spectrum of NGC 5548 at two epochs, when the source was bright (*continuous line*) and when it was faint (*dashed line*). The faint-state spectrum is the unweighted mean of SWP 35617, 35636, 35676, 35677, and 35712. The bright-state spectrum is the unweighted mean of SWP 36089, 36159, 36160, and 36184. The corresponding mean Julian Dates are 2,447,588 and 2,447,646, respectively. The positions of the strongest emission lines are indicated.

b) Gaussian Extraction of Data, and Line and Continuum Fitting

In order to enhance the signal-to-noise ratio (S/N) and thereby bring out the weaker emission lines, an optimal spec-
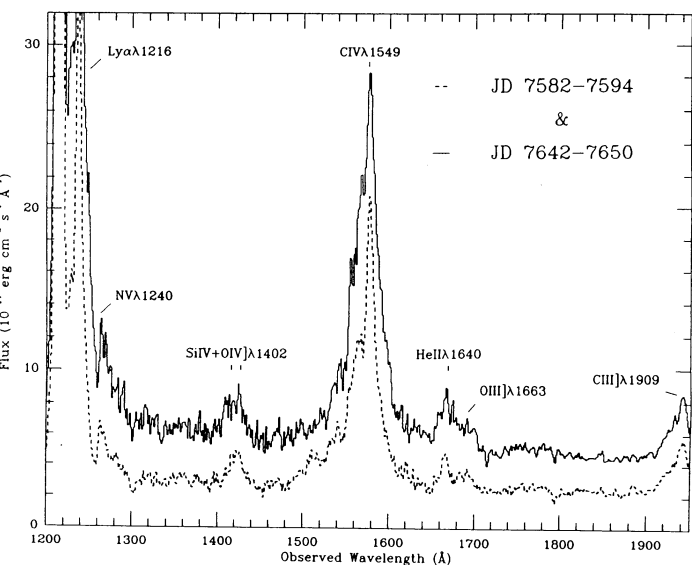
tral extraction method was also applied to the data. The inputs to the procedure were the two-dimensional, geometrically and photometrically corrected ELBL files as processed by the standard IUESIPS software. Prior to the extraction, the images were cleaned of cosmic-ray hits and other blemishes. The background regions on either side of the spectrum were cleaned by calculating the flux percentiles within smaller regions, and replacing the fluxes which fell outside the upper or lower 2 percentiles by the median values. Blemishes in the source region were removed interactively by interpolation over the affected pixels.

The optimal extraction method used was a modified version of the Gaussian extraction (GEX) technique. Details concerning the standard GEX technique are given in the discussion by Urry and Reichert (1988). Briefly, the two-dimensional data are summed over bins in wavelength, and each binned cross-dispersive profile is fitted to a Gaussian point-spread function (PSF) plus a linear background. Two passes through the data are made. In the first pass, large wavelength bins are used, and the background and Gaussian parameters are all allowed to vary freely. In the second pass the data are summed over smaller wavelength bins, and only the normalizations of the Gaussians are allowed to vary. All other parameters are determined from the larger bin values, either by fitting to a quadratic dependence on wavelength or by linear interpolation. The net spectral fluxes are given by the integrals under the Gaussian fits to the smaller bins.

The version of GEX used in this work incorporates several improvements over the standard GEX, taking advantage of a better knowledge of the *IUE* camera's PSFs and the varying S/N in the NGC 5548 spectra. Details concerning the necessity of the improvements and their implementation are given by Reichert and Kriss (1990). The modifications are as follows: (1) Cassatella, Barbero, and Benvenuti (1985, hereafter CBB) have shown that the PSF in the SWP camera is better fitted by a skewed Gaussian than by a symmetrical Gaussian. The procedure was therefore modified to fit skewed Gaussians to the cross-dispersive SWP profiles, with the skew parameters fixed according to the curve determined by CBB. (2) The procedure was modified to allow the cross-dispersive profiles to be summed over bins of variable width, so that comparatively wide bins could be used for the continuum regions and regions of lower camera sensitivity, and narrower bins used for the emission lines and regions of higher camera sensitivity. (3) The Gaussian widths for the second pass through the data were determined by higher order polynomial fits to the first-pass values. Fourth-order polynomials were fitted to the SWP widths, while fifth-order polynomials were used for the LWP widths. (4) Finally, the conversion from net to absolute spectral fluxes was calibrated using fits to bright standard stars.

In the absence of a true noise model for *IUE* data, it can be difficult to derive true uncertainties for the extracted fluxes. However, assuming that the fitted Gaussians (or skewed Gaussians) are good representations of the cross-dispersive profiles, and barring systematic effects, then the deviations between the fitted models and the data should give a measure of the uncertainties. We have therefore adopted the deviation between the fitted model and the data as an estimate of the *statistical* uncertainty associated with each flux. The advantage of this method is that it allows independent estimates of the flux uncertainties to be determined for each flux, and can be used for the majority of epochs when only one spectrum per camera was obtained.

As a check on this method of estimating uncertainties, we have also estimated uncertainties by averaging near-concurrent spectra on a pixel-by-pixel basis, and computing the residuals about these averages. By repeating this process for a number of spectral pairs, we derived distributions of residuals at various wavelengths for each camera. The widths of the distributions are measures of the uncertainties. In every case, the uncertainties derived from the GEX fits to the cross-dispersive profiles closely matched the widths of the distributions of residuals, supporting our use of the GEX uncertainties. Further justifications of the GEX uncertainties are discussed by Reichert and Kriss (1990).

We note that the GEX uncertainties should be considered purely statistical uncertainties, and as such probably do not include systematic uncertainties such as those due to fixed pattern noise, etc. (The residuals from the spectral pairs will also not include systematic uncertainties.) It is well established that *IUE* data are subject to systematic uncertainties (see, e.g., Bohlin 1988), and this fact probably accounts for the high values of reduced χ^2 derived from the fits to continuum and emission-line regions (see discussion below). Based on the results of these fits, we deduce that our estimated uncertainties represent approximately half of the combined statistical plus systematic uncertainties.

Emission-line and continuum fluxes in the GEX–extracted spectra are derived from multicomponent, least-squares fits to the data. Full details of the fitting procedure will be described in Reichert and Kriss (1990). Here we give a brief summary of the major steps.

For the SWP spectra, parameters in the least-squares fits include a power law of the form

$$F_\lambda = F_0\left(\frac{\lambda}{1000}\right)^{-\beta},$$

plus 14 Gaussian components: two for Lyα, five for C IV λ1549, two for C III] λ1909, one each for N V λ1240, O I λ1304, Si IV + O IV] λ1402, and He II λ1640 + O III] λ1663, and one in optical depth for the N V λ1240 absorption feature. Each Gaussian component has its total flux, central wavelength, and its dispersion as free parameters. No physical significance is attached to any of these components. They merely serve as a convenient description of the data which permit accurate fluxes with suitable error bars to be determined.

Fits to the SWP spectra are done in a stepwise fashion that decouples parameters that are not closely linked. Starting from a fit to an average spectrum, initial guesses for the line and continuum fluxes are made by scaling this fit by previously determined quick-look answers for the continuum flux at 1337 Å and the C IV flux. The continuum is then fitted in the line-free windows 1317–1357 Å plus 1720–1858 Å. With the continuum fixed, the Si IV + O IV blend, the C III] line, and the C IV and He II + O III] region are all fitted individually. Once initial fits have been made to each of these independent line complexes, the spectral range from 1350 to 1962 Å (observed wavelengths) is fitted with all line and continuum parameters free to vary. A 7 Å region surrounding the camera feature at λ_{obs} = 1666 Å and a 9 Å region around the reseau at λ_{obs} = 1799 Å are excluded from the final fit.

Lines in the Lyα region are fitted independently with the continuum fixed according to the fits redward of 1337 Å, since there is no good continuum shortward of Lyα. An initial fit is performed with the width of broad Lyα and N V fixed. This

yields better consistency in the final answers. After this iteration establishes the line fluxes and centers, a final fit is done in which all line components are allowed to vary freely.

Fits to the LWP spectra are complicated by the pseudocontinuum of Fe II emission, which is present throughout the LWP spectral range (see § IIIa). To avoid the complications of modeling the entire Fe II spectrum, only a small region around Mg II from 2540 to 3050 Å is fitted. The window from $\lambda_{obs} = 3035$ Å to $\lambda_{obs} = 3075$ Å is excluded to avoid a reseau. Strong blends of Fe II emission are modeled with broad Gaussians centered at 2595, 2724, and 2947 Å. The underlying pseudocontinuum of weaker Fe II lines and Balmer continuous emission is fitted with a power law. Comparing an average of all LWP spectrum to a model of Fe II emission (Netzer and Wills 1983) shows that the 2645–2695 Å wavelength interval represents a local minimum in the Fe II emission. It was therefore chosen to sample the continuum in the LWP. A single Gaussian describes the profile of Mg II $\lambda2798$ well if an additional Gaussian is included to account for the bright Fe II feature at 2838 Å in the models of Netzer and Wills (1983).

In fitting an individual LWP spectrum, the Fe II line fluxes are fixed, and the continuum parameters are adjusted using a wavelength range which avoids the Mg II line. Next, the continuum is fixed, and only the line fluxes are permitted to vary. In the final iteration all parameters are permitted to vary freely.

Error bars for the fitted parameters in both the SWP and the LWP spectra are calculated in a semiempirical way. Under the assumption that each parameter is a single "interesting" parameter (see Avni 1976), the 1 σ error σ_i on a parameter a_i is obtained from the error matrix of the fit, ϵ_{ij}, scaled by the reduced chi-square, χ_v^2:

$$\sigma_i^2 = \chi_v^2 \epsilon_{ii} .$$

For observed quantities of interest which are functions of more than one parameter, e.g., the total flux of C IV, the error bar is calculated using

$$\sigma_{\text{C IV tot}}^2 = \sum_i \sigma_i^2 + \sum_{i \neq j} \sigma_{ij}^2 ,$$

where the cross-variance σ_{ij}^2 is the error matrix element ϵ_{ij} scaled by χ_v^2. Typically, χ_v^2 for the final fits ranged from 3 to 5, indicating that the statistical uncertainties for the individual fluxes (derived from the deviations about the cross-dispersive profiles in the Gaussian extractions) probably underestimate the combined uncertainties by a factor of ~ 2.

We tested the appropriateness of the errors in the line and continuum fluxes by examining the scatter in the results for multiple observations. For the SWP we use pairs of spectra that were obtained during the same IUE shift. For the LWP we used adjacent pairs of spectra, since only one pair of LWP exposures were taken on the same shift. Under the assumption that there is no variability on such short time scales, the differences in line or continuum flux for the spectral pairs, divided by the estimated errors summed in quadrature, should show a Gaussian distribution with zero mean and unit dispersion if the error bars are appropriate and if there are no external sources of error. The distributions of the scaled differences for the fluxes have dispersions of ~ 2 for C IV and Si IV, ~ 5 for Lyα, N V, He II, C III], and F_{1813}, and ~ 7 for F_{1337}. Thus, while the calculated errors are probably accurate measures of the statistical errors internal to a given spectrum, they do not assess the true external errors for the repeatability of IUE spectra. To account for these additional external errors, the tabulated errors for the final results were therefore scaled up by

a factor equal to the dispersions measured for the scaled difference distributions of the spectral pairs.

c) Comparison of Results

In what follows, we shall refer to the IUESIPS data extraction plus flux summation method as SIPS, whereas the Gaussian extraction plus line and continuum fitting process will be called GEX, for simplicity.

The continuum flux at 1350 Å (SIPS), 1337 Å (GEX) 1840 Å (SIPS), and 1813 Å (GEX), the SWP frequency spectral index α ($F_v \propto v^{-\alpha}$), as well as the Lyα $\lambda1216$ + N V $\lambda1240$ blend and C IV $\lambda1549$ line fluxes measured both with SIPS and GEX, are listed in Table 2. We caution that the values of α listed slightly overestimate the true spectral index of the continuum, since no attempt has been made to remove the steep pseudocontinuum created by the many blended low-contrast Fe II lines and Balmer continuum emission (Wills, Netzer, and Wills 1985). In Table 3 we give the SIPS and GEX fluxes of Si IV + O IV] $\lambda1402$, He II $\lambda1640$ + O III] $\lambda1663$, C III] $\lambda1909$, and N V $\lambda1240$ (GEX only). Table 4 contains the 2670 Å continuum and Mg II $\lambda2798$ line SIPS and GEX fluxes. All fluxes are given as a function of the Julian Date and time at the start of the corresponding exposure.

Knowing the width of the IUE point-spread function and its wavelength dependence (CBB), it is possible to estimate the fraction of the flux which actually entered the spectrographs on 1989 February 8 and correct for the effect of vignetting. The correction factors which have been applied to each of the line and continuum fluxes are given in the footnotes to the tables. Because of their systematic uncertainty, however, the data of 1989 February 8 have not been included in the analysis of §§ IV and V. We checked, however, that their inclusion does not affect any of the results.

For time series analysis it is convenient to have only one flux measurement per epoch. The results obtained during the same observing shift were therefore averaged. In the case of the data reduced with SIPS, the averaging was performed after extraction of the individual line and continuum fluxes by computing their weighted mean. For the GEX data, the spectra obtained on the same day are first averaged using a weighted mean, and the fitting procedure is performed again on the mean spectra to measure the line and continuum fluxes and their associated errors. In the remainder of this paper, we shall be concerned with the averaged results only.

To compare the results obtained with SIPS and GEX, linear regression analysis was performed between both sets of measurements. The regression techniques used take into account the errors both on the dependent (GEX) and the independent (SIPS) variable simultaneously (York 1966). The results are given in Table 5, where we list the coefficients of the best-fit regression line, the correlation coefficient, the reduced chi-square, and the probability of exceeding χ_v^2 by chance. In Figure 2 the GEX fluxes are plotted as a function of their SIPS counterpart for F_{1337} and F_{1350}, C IV $\lambda1549$, and He II $\lambda1640$ + O III] $\lambda1663$. The agreement between the two data sets is excellent. The correlation coefficients r and reduced chi-squares are always highly significant. For the continuum fluxes, the χ_v^2 values are significantly smaller than 0.5. This is partly because the two methods are not statistically independent, nearly identical quantities being derived from the same data. In addition, the errors which enter into the calculation of χ_v^2 include both internal statistical errors and external system-

TABLE 2

SWP Observations

J.D. (-2,440,000)	F_{1350} SIPS	F_{1337} GEX $(10^{-14} \mathrm{erg\ s^{-1}cm^{-2}\AA^{-1}})$	F_{1840} SIPS	F_{1813} GEX	α_ν GEX	Ly$\alpha\lambda$1216+NVλ1240 SIPS	GEX $(10^{-14}\mathrm{erg\ s^{-1}cm^{-2}})$	CIVλ1549 SIPS	GEX
7510.139	3.71±0.26	3.63±0.12	2.95±0.18	3.02±0.08	1.40±0.11	456±17.	654±41.	638±23.	613±31
7514.082	4.03±0.26	4.00±0.15	3.04±0.18	2.99±0.08	1.05±0.12	493±17.	661±55.	717±23.	684±42
7517.926	4.21±0.26	4.23±0.13	3.19±0.18	3.23±0.07	1.12±0.10	504±17.	670±50.	694±23.	668±25
7522.091	4.10±0.26	4.78±0.16	3.54±0.18	3.70±0.09	1.16±0.11	530±17.	730±59.	740±23.	727±30
7526.099	5.10±0.26	5.16±0.18	3.58±0.18	3.59±0.10	0.82±0.12	555±17.	663±57.	691±23.	673±35
7530.013	5.32±0.26	5.18±0.16	3.77±0.18	3.76±0.09	0.94±0.10	553±17.	769±60.	677±23.	662±24
7534.002	5.00±0.26	4.99±0.15	3.54±0.18	3.64±0.09	0.97±0.10	488±17.	682±63.	643±23.	636±28
7538.170	6.14±0.26	6.07±0.17	4.27±0.18	4.27±0.09	0.85±0.09	601±17.	838±70.	701±23.	660±25
7538.265	5.89±0.26	6.05±0.17	4.46±0.18	4.38±0.09	0.94±0.09	601±17.	844±64.	727±23.	689±25
7538.355	5.89±0.26	6.07±0.17	4.71±0.18	4.37±0.09	0.92±0.09	654±17.	932±82.	705±23.	735±28
7543.214	6.23±0.26	6.38±0.21	4.60±0.18	4.53±0.11	0.87±0.11	619±17.	943±64.	765±23.	760±44
7543.306	5.78±0.26	6.20±0.20	4.47±0.18	4.59±0.12	1.01±0.11	656±17.	884±67.	760±23.	710±38
7546.009	6.28±0.26	6.14±0.17	4.52±0.18	4.51±0.10	0.99±0.09	670±17.	932±61.	786±23.	765±35
7549.831	5.24±0.26	5.24±0.16	3.83±0.18	3.95±0.09	1.08±0.10	649±17.	937±57.	796±23.	774±22
7553.160	4.93±0.26	5.11±0.19	3.80±0.18	3.90±0.11	1.11±0.12	660±17.	799±56.	892±23.	863±50
7557.159	4.76±0.26	4.67±0.18	3.40±0.18	3.61±0.11	1.16±0.13	626±17.	801±52.	795±23.	807±27
7557.244	4.96±0.26	4.80±0.19	3.45±0.18	3.48±0.10	0.94±0.13	636±17.	807±59.	785±23.	763±33
7561.855	3.55±0.26	3.36±0.14	2.80±0.18	2.75±0.09	1.34±0.13	545±17.	720±51.	715±23.	736±39
7565.871[a]	2.99±0.26	2.97±0.14	2.90±0.18	2.71±0.07	1.41±0.16	479±17.	812±50.	656±23.	633±24
7569.845	3.28±0.26	3.22±0.13	2.56±0.18	2.55±0.08	1.23±0.13	511±17.	651±50.	654±23.	672±53
7573.713	3.00±0.26	3.15±0.13	2.25±0.18	2.33±0.07	1.02±0.13	475±17.	571±50.	622±23.	619±23
7577.919	2.88±0.26	2.53±0.16	2.29±0.18	2.18±0.11	1.52±0.21	445±17.	546±47.	656±23.	600±33
7581.866	2.55±0.26	2.54±0.12	2.11±0.18	2.08±0.08	1.35±0.16	414±17.	544±43.	547±23.	541±20
7586.013	3.50±0.26	3.34±0.11	2.59±0.18	2.61±0.07	1.19±0.11	425±17.	579±49.	582±23.	588±18
7586.107	2.83±0.39	2.66±0.21	2.10±0.27	2.13±0.13	1.28±0.25	400±26.	497±47.	583±35.	510±47
7589.991	3.19±0.26	3.10±0.14	2.40±0.18	2.46±0.08	1.24±0.14	432±17.	505±29.	596±23.	602±21
7590.089	2.60±0.26	2.81±0.19	2.18±0.18	2.32±0.12	1.37±0.22	421±17.	563±48.	599±23.	614±11
7594.001	2.97±0.26	3.13±0.13	2.47±0.18	2.46±0.08	1.20±0.14	454±17.	594±47.	585±23.	594±13
7594.101	2.91±0.26	2.75±0.21	2.11±0.18	2.22±0.13	1.31±0.24	428±17.	487±56.	644±23.	584±29
7597.998	4.18±0.26	4.04±0.18	2.90±0.18	3.02±0.10	1.04±0.14	422±17.	527±37.	594±23.	557±10
7598.090	3.62±0.26	3.73±0.22	2.63±0.18	2.83±0.13	1.09±0.20	453±17.	538±58.	627±23.	555±58
7601.997	4.40±0.26	4.60±0.17	3.32±0.18	3.31±0.10	0.92±0.13	447±17.	583±56.	593±23.	556±18
7602.095	4.20±0.26	4.08±0.16	3.23±0.18	3.33±0.10	1.34±0.13	456±17.	633±53.	625±23.	619±27
7606.010	4.46±0.26	4.43±0.16	3.43±0.18	3.47±0.10	1.19±0.12	453±17.	615±54.	612±23.	616±24
7606.103	3.90±0.39	3.78±0.23	3.23±0.27	3.07±0.14	1.32±0.20	450±26.	699±60.	642±35.	664±32
7609.905	4.82±0.26	4.76±0.62	3.98±0.18	3.51±0.11	1.00±0.12	483±17.	680±52.	580±23.	632±21
7613.685	5.29±0.26	5.42±0.15	3.97±0.18	3.98±0.08	0.99±0.09	516±17.	745±59.	684±23.	669±20
7617.623	5.30±0.26	5.31±0.14	3.75±0.18	3.80±0.08	0.90±0.09	503±17.	709±45.	668±23.	700±11
7621.588	7.09±0.26	7.17±0.20	4.70±0.18	4.89±0.10	0.74±0.09	590±17.	794±55.	745±23.	748±16
7625.591	6.46±0.26	6.86±0.16	4.63±0.18	4.76±0.08	0.80±0.08	602±17.	898±68.	769±23.	772±12
7629.740	6.91±0.26	6.91±0.18	4.73±0.18	4.83±0.10	0.83±0.09	603±17.	874±72.	776±23.	759±22
7629.845	6.63±0.26	6.41±0.32	4.61±0.18	4.68±0.18	0.96±0.16	591±17.	989±73.	738±23.	716±28
7633.926	6.43±0.26	6.50±0.19	4.80±0.18	4.73±0.10	0.96±0.10	672±17.	997±76.	755±23.	741±19
7634.017	6.11±0.39	6.21±0.29	4.10±0.27	4.33±0.16	0.82±0.16	592±26.	706±84.	771±35.	727±35
7637.916	6.28±0.26	6.37±0.21	4.42±0.18	4.57±0.12	0.91±0.11	707±17.	955±77.	789±23.	778±43

atic uncertainties, whereas only the internal errors are relevant when comparing the GEX and SIPS results.

Apart from the He II λ1640 and Lyα λ1216 lines, the slope of the best-fit regression lines never differs from unity by more than 2 σ, while the intercepts are null to within the error bars. The GEX fluxes for Lyα λ1216 are systematically larger by ~50% than the SIPS values. This is a direct consequence of the fitting procedure which "restores" part of the blue wing

occulted under the geocoronal emission feature. The GEX measurements of the He II λ1640 + O III] λ1663 blend are almost twice as large as their SIPS counterpart. This difference appears to be primarily due to the way the fitting procedure deblends the He II λ1640 + O III] λ1663 feature from the broad red wing of the C IV λ1549 line. The SIPS integration interval is chosen to be symmetrical about 1640 Å, with a width determined from the local minimum of the flux in the interval

TABLE 2—*Continued*

J.D. (-2,440,000)	F_{1350} SIPS	F_{1337} GEX	F_{1840} SIPS	F_{1813} GEX	α_ν GEX	Ly$\alpha\lambda$1216+NVλ1240 SIPS	GEX	CIVλ1549 SIPS	GEX
		(10^{-14}erg s^{-1}cm^{-2}Å^{-1})				(10^{-14}erg s^{-1}cm^{-2})			
7638.012	5.94±0.26	5.99±0.34	4.27±0.18	4.41±0.10	1.00±0.14	609±17.	792±70.	757±23.	697±49
7641.981	6.56±0.26	6.70±0.20	5.02±0.18	5.01±0.11	1.05±0.10	728±17.	1033±79.	834±23.	767±33
7645.906	6.46±0.26	6.53±0.21	4.26±0.18	4.61±0.11	0.86±0.11	757±17.	1069±80.	907±23.	832±41
7645.993	6.24±0.26	6.60±0.22	4.50±0.18	4.53±0.12	0.77±0.11	725±17.	1073±81.	849±23.	846±44
7649.840	5.82±0.26	5.88±0.21	4.33±0.18	4.35±0.12	1.02±0.11	757±17.	1066±84.	855±23.	831±40
7649.935	5.38±0.39	5.49±0.33	3.90±0.27	3.96±0.18	0.92±0.20	735±26.	1076±92.	846±35.	800±54
7653.850	5.69±0.26	5.74±0.19	4.23±0.18	4.31±0.11	1.06±0.11	729±17.	943±65.	871±23.	879±29
7657.524	5.18±0.26	5.26±0.16	4.25±0.18	4.04±0.10	1.13±0.10	707±17.	1076±83.	865±23.	854±25
7661.502	5.05±0.26	5.17±0.19	3.98±0.18	3.89±0.11	1.07±0.12	682±17.	967±62.	834±23.	853±27
7665.495	5.26±0.26	5.34±0.17	3.78±0.18	3.85±0.09	0.93±0.11	674±17.	924±71.	844±23.	799±35
7669.502	4.23±0.26	4.29±0.16	3.37±0.18	3.42±0.10	1.26±0.12	655±17.	992±74.	818±23.	805±38
7669.599	4.28±0.26	4.29±0.18	3.54±0.18	3.46±0.11	1.30±0.14	668±17.	856±59.	836±23.	798±39
7673.551	4.20±0.26	4.07±0.13	3.36±0.18	3.32±0.08	1.33±0.11	651±17.	885±55.	849±23.	834±29
7677.519	3.76±0.26	3.62±0.15	3.13±0.18	3.12±0.10	1.51±0.13	613±17.	912±62.	823±23.	841±35
7680.745	4.34±0.26	4.29±0.19	3.23±0.18	3.16±0.10	1.00±0.14	592±17.	822±55.	805±23.	787±39
7680.852	3.60±0.39	3.37±0.19	3.08±0.27	3.03±0.13	1.65±0.19	587±26.	824±69.	753±35.	772±48
7684.929	3.68±0.26	3.63±0.13	3.01±0.18	2.95±0.08	1.33±0.11	578±17.	807±51.	780±23.	765±27
7685.019	3.03±0.39	3.10±0.21	2.55±0.27	2.55±0.13	1.36±0.23	567±26.	674±56.	767±35.	726±44
7688.742	3.17±0.26	3.14±0.14	2.69±0.18	2.57±0.09	1.34±0.15	513±17.	686±52.	723±23.	713±30
7688.840	2.89±0.26	2.62±0.16	2.46±0.18	2.50±0.11	1.85±0.19	497±17.	685±54.	677±23.	657±36
7692.743	3.22±0.26	3.05±0.14	2.67±0.18	2.59±0.09	1.46±0.15	492±17.	675±52.	725±23.	684±39
7692.843	3.24±0.26	2.67±0.17	2.71±0.18	2.57±0.13	1.87±0.21	472±17.	689±56.	651±23.	627±44
7696.757	3.20±0.26	3.30±0.11	2.67±0.18	2.73±0.07	1.39±0.11	499±17.	655±47.	644±23.	675±33
7700.740	3.48±0.26	3.57±0.13	2.81±0.18	2.81±0.08	1.22±0.12	503±17.	646±44.	668±23.	652±26
7700.839	3.06±0.26	3.23±0.19	2.41±0.18	2.51±0.11	1.18±0.19	450±17.	651±48.	690±23.	657±34
7705.430	3.56±0.26	3.54±0.14	2.76±0.18	2.86±0.09	1.31±0.13	520±17.	692±47.	665±23.	698±26
7709.340	4.47±0.26	4.51±0.15	3.35±0.18	3.29±0.08	0.96±0.11	578±17.	781±78.	699±23.	722±28
7713.335	4.41±0.26	4.34±0.15	3.25±0.18	3.25±0.09	1.06±0.11	574±17.	806±56.	790±23.	755±27
7717.323	4.40±0.26	4.44±0.16	3.42±0.18	3.44±0.10	1.16±0.12	634±17.	852±53.	823±23.	781±29
7721.335	4.80±0.26	4.72±0.19	3.29±0.18	3.35±0.10	0.87±0.13	611±17.	828±73.	856±23.	791±35
7725.337	4.16±0.26	4.12±0.16	2.91±0.18	3.03±0.09	0.99±0.13	613±17.	785±64.	874±23.	868±32
7725.436	3.48±0.39	3.22±0.22	2.81±0.27	2.74±0.14	1.48±0.22	600±26.	885±68.	810±35.	861±47
7729.670	2.81±0.26	2.63±0.13	2.37±0.18	2.32±0.09	1.59±0.16	549±17.	787±57.	822±23.	799±24
7729.768	2.29±0.39	2.61±0.25	2.01±0.27	1.91±0.14	0.97±0.31	538±26.	692±53.	773±35.	708±52
7733.680	2.21±0.26	2.11±0.12	1.98±0.18	1.93±0.09	1.71±0.19	459±17.	721±47.	658±23.	646±24
7733.775	2.08±0.39	2.19±0.24	1.79±0.27	1.58±0.13	0.93±0.36	453±26.	449±52.	558±35.	522±43
7737.662	1.68±0.26	1.59±0.09	1.60±0.18	1.55±0.07	1.90±0.18	407±17.	523±40.	496±23.	514±26
7737.759	1.50±0.26	1.52±0.13	1.31±0.18	1.35±0.09	1.61±0.28	397±17.	443±45.	526±23.	508±31
7741.582	1.73±0.26	1.64±0.10	1.70±0.18	1.56±0.07	1.83±0.20	388±17.	503±32.	466±23.	469±26
7745.557	1.88±0.26	1.77±0.09	1.65±0.18	1.67±0.06	1.81±0.16	396±17.	568±40.	475±23.	481±24

[a] Vignetting correction factors: F_{1350} and F_{1337}, 1.28; F_{1840} and F_{1813}, 1.41; Lyα, 1.31; C IV, 1.33.

between the He II and the C IV lines. Because the C IV λ1549 wings overwhelm those of He II λ1640 in that range, the SIPS interval therefore underestimates the true extent of the He II feature. As pointed out by Wamsteker et al. (1990), the very broad wings of He II λ1640 are particularly strong in NGC 5548 and dominate the total line emission. This explains why the GEX fits, which recover a fraction of the flux in the wing from the region where it is blended with C IV λ1549, yield systematically larger He II intensities than SIPS.

IV. THE PATTERN OF VARIABILITY

Before discussing the variability, we set out the mean properties of NGC 5548's ultraviolet spectrum as determined by our monitoring. The average line and continuum fluxes are listed in Table 6.

The average spectral index for the power-law fit to the SWP spectrum ($F_\nu \propto \nu^{-\alpha}$) is $\langle\alpha\rangle \simeq 1.17$. Correction for Galactic reddening ($E_{B-V} = 0.05$; Wamsteker et al. 1990) brings this value to $\simeq 0.95$. The *intrinsic* continuum in NGC 5548 may be slightly flatter, however. As mentioned in § IIIa, blended low-contrast Fe II lines create an artificial continuum whose intensity decreases rapidly with wavelength but which still contributes about 10% to the average flux at 1840 Å. After removal of the Fe II line spectrum and Balmer continuum emission, Wamsteker et al. (1990) found a mean spectral index $\langle\alpha\rangle \simeq 0.39$ for the NGC 5548 energy distribution, from the

TABLE 3

WEAK EMISSION LINES

J.D. (-2,440,000)	SiIV+OIV]λ1402		HeIIλ1640[a]		CIII]λ1909		NVλ1240
	SIPS	GEX	SIPS	GEX	SIPS	GEX	GEX
			(10^{-14} erg s^{-1} cm^{-2})				
7510.139	37±11	45± 7	43±10	58±19	92±15	74± 8	94±20
7514.082	50±11	48±11	64±10	68±15	116±15	95±10	104±25
7517.926	47±11	42± 7	46±10	88±22	118±15	90± 8	90±22
7522.091	65±11	55±10	61±10	88±12	117±15	78± 9	<133±32
7526.099	45±11	40± 9	74±10	108±16	118±15	107±11	82±30
7530.013	28±11	42± 8	58±10	97±15	94±15	84±10	108±27
7534.002	28±11	47± 9	73±10	99±16	127±15	98±10	82±27
7538.170	38±11	65± 9	65±10	109±15	120±15	94±11	111±34
7538.265	58±11	43±11	97±10	133±16	109±15	84±10	192±34
7538.355	48±11	62±11	72±10	120±14	86±15	99±12	161±41
7543.214	37±11	35± 9	76±10	108±15	113±15	91±13	132±30
7543.306	62±11	56±13	88±10	117±19	139±15	104±13	122±33
7546.009	49±11	55±10	93±10	114±14	90±15	92±14	180±30
7549.831	62±11	70±11	82±10	128±15	120±15	103±10	163±23
7553.160	74±11	73±13	81±10	108±15	112±15	88±10	107±33
7557.159	59±11	79±12	81±10	74±12	158±15	109±10	64±23
7557.244	49±11	55±13	65±10	67±13	147±15	122±17	112±34
7561.855	42±11	54± 9	42±10	49± 9	130±15	117±10	63±23
7565.871[b]	56±11	63±10	44±10	62±11	153±15	133± 8	109±25
7569.845	40±11	49± 8	62±10	68± 8	136±15	119±10	76±22
7573.713	37±11	37± 7	51±10	54± 6	136±15	105± 8	4±17
7577.919	51±11	42± 8	45±10	32±11	106±15	98±10	37±30
7581.866	29±11	27± 7	39±10	36± 6	128±15	106± 7	9±18
7586.013	32±11	34± 6	45±10	49± 6	88±15	70± 5	65±21
7586.107	43±17	28±13	69±15	91±12	138±23	118±16	39±22
7589.991	36±11	43± 6	47±10	37± 6	121±15	91± 6	87±20
7590.089	52±11	52±13	45±10	37± 6	92±15	104±13	68±29
7594.001	28±11	38± 7	56±10	55± 6	95±15	103± 8	30±21
7594.101	51±11	53±17	91±10	50± 8	113±15	86±11	96±37
7597.998	30±11	34±12	70±10	63± 7	84±15	68± 9	61±19
7598.090	50±11	44±13	76±10	43± 7	116±15	86±11	97±40
7601.997	41±11	36± 8	56±10	66± 7	64±15	63± 7	37±26
7602.095	45±11	44± 9	56±10	58± 6	99±15	89± 9	92±27
7606.010	25±11	60±11	50±10	59± 7	78±15	68± 8	20±21
7606.103	37±17	63±15	31±15	30± 5	124±23	96±10	139±42
7609.905	45±11	47±13	77±10	89± 8	89±15	97±10	59±21
7613.685	57±11	61± 9	72±10	104± 2	105±15	80± 8	106±28
7617.623	40±11	63± 8	56±10	76± 5	100±15	96± 8	23±25
7621.588	26±11	49±10	62±10	88±13	112±15	84± 8	181±32
7625.591	59±11	73±11	56±10	97± 5	126±15	96± 9	132±42
7629.740	52±11	70±12	70±10	89±17	117±15	97±11	120±38
7629.845	53±11	74±21	56±10	75± 5	72±15	86±13	155±44
7633.926	63±11	71±11	77±10	92± 6	105±15	96± 9	100±38
7634.017	48±17	31±19	69±15	52± 6	144±23	136±18	145±51
7637.916	55±11	60±11	79±10	88±20	122±15	97±12	82±37

optical to the ultraviolet. The contamination by Fe II lines is even greater in the LWP band, making it futile to attempt a description of the continuum shape there.

The ultraviolet spectrum of NGC 5548 varied significantly during the observing campaign. This is clearly illustrated by Figure 1, where the mean SWP spectrum during the local minimum of late February to early March is plotted on the same scale as the mean SWP spectrum 2 months later, when the continuum and line fluxes reached a maximum.

The light curves of the continuum flux, the FES, and the strong C IV λ1549 and Lyα λ1216 emission lines are shown in Figure 3, whereas those of the other lines appear in Figure 4. Apart from the N V λ1240 line, these figures were generated from the SIPS measurements. It is obvious from these curves

TABLE 3—Continued

| J.D. (-2,440,000) | SiIV+OIV]λ1402 | | HeIIλ1640[a] | | CIII]λ1909 | | NVλ1240 |
| | SIPS | GEX | SIPS | GEX | SIPS | GEX | GEX |
			(10^{-14} erg s^{-1} cm^{-2})				
7638.012	74±11	82±19	81±10	88± 5	123±15	106±14	6±39
7641.981	52±11	50±11	93±10	103±23	112±15	85±10	100±34
7645.906	58±11	66±14	115±10	113± 4	137±15	90±11	165±40
7645.993	52±11	69±12	76±10	105±10	142±15	127±10	86±48
7649.840	51±11	56±10	101±10	115± 6	137±15	106±12	164±42
7649.935	72±17	78±22	83±15	80± 4	121±23	115±19	272±50
7653.850	53±11	69±11	84±10	119±10	110±15	103±12	67±25
7657.524	71±11	81± 8	81±10	121± 8	126±15	121±10	153±31
7661.502	68±11	92±11	84±10	137±10	136±15	150±18	122±28
7665.495	61±11	55± 9	70±10	94±29	127±15	104±10	97±32
7669.502	69±11	61±10	82±10	107± 2	146±15	133±11	147±28
7669.599	88±11	74±14	77±10	88±37	133±15	111±10	37±29
7673.551	62±11	74±10	66±10	88± 6	127±15	115±10	92±29
7677.519	66±11	93±11	71±10	79±14	137±15	105±11	144±27
7680.745	57±11	58±10	66±10	63± 2	140±15	126±12	53±20
7680.852	30±17	67±19	90±15	107± 6	152±23	123±13	85±33
7684.929	67±11	67± 8	61±10	70± 5	141±15	126±10	111±25
7685.019	69±17	62±13	48±15	47±14	153±23	153±17	105±29
7688.742	61±11	66±10	33±10	42± 5	125±15	117±10	42±23
7688.840	47±11	50±13	55±10	38± 6	149±15	132±13	56±31
7692.743	57±11	72±10	59±10	46± 4	120±15	101± 9	68±19
7692.843	39±11	59±14	37±10	33±16	129±15	112±15	98±29
7696.757	44±11	54± 9	37±10	46±24	112±15	98± 9	41±25
7700.740	36±11	34± 8	48±10	53± 2	105±15	92± 8	30±23
7700.839	65±11	66±13	39±10	57±32	137±15	118±11	66±23
7705.430	45±11	59± 9	56±10	65± 9	127±15	100±10	75±23
7709.340	40±11	51± 9	58±10	78± 5	112±15	102±10	75±27
7713.335	66±11	70±10	71±10	97± 7	146±15	106±10	101±28
7717.323	51±11	57± 9	86±10	109±40	121±15	100±11	101±25
7721.335	54±11	58± 8	81±10	75± 2	105±15	108±14	94±27
7725.337	50±11	75± 9	72±10	105±23	140±15	108±10	45±23
7725.436	66±17	85±17	74±15	102± 6	131±23	126±20	139±42
7729.670	60±11	67±10	62±10	62± 7	116±15	107± 8	52±28
7729.768	44±17	43±18	63±15	55±25	144±23	140±17	71±27
7733.680	56±11	72±11	33±10	28± 4	135±15	113±25	62±24
7733.775	23±17	28±14	39±15	38±42	137±23	135±18	110±38
7737.662	32±11	41± 7	35±10	22± 1	126±15	99± 8	0±18
7737.759	43±11	42±10	52±10	26±23	129±15	116±10	53±21
7741.582	43±11	50± 8	24±10	27± 2	82±15	80± 7	40±14
7745.557	33±11	48± 7	30±10	18± 7	112±15	81± 6	18±18

[a] Includes also O III] λ1663.
[b] Vignetting correction factors: Si IV, 1.29; He II, 1.34; C III, 1.37; N V, 1.31.

that significant changes were observed in all these quantities, and that the dominant time scale of variation (i.e., the "pseudoperiod") was ~ 80 days.

Table 6 summarizes the main characteristics of the variability for each of the quantities we measured: its mean value over the entire period of observations, the fractional variation F_{var} defined as the ratio of the rms fluctuation to the mean flux, and the ratio of maximum to minimum flux, R_{max}. The fractional variations have been corrected to represent the intrinsic variations by subtracting the mean measuring error for the feature in quadrature. Except for N v $\lambda1240$, both the SIPS and the

GEX values are listed. Again, the agreement between the two methods is excellent, there being no systematic differences apart from those already noted which affect the Lyα $\lambda1240$ and He II $\lambda1640$ fluxes.

The longer the wavelength, the smaller the amplitude of the continuum variations. F_{var} decreases gradually from $\simeq 0.30$ at 1350 Å to 0.26 at 1840 Å, 0.16 at 2670 Å, and 0.08 near 5000 Å (FES). Since the variations are simultaneous in all three bands (see Table 7), this implies that the spectrum becomes systematically bluer when it gets brighter. The large dilution of the nuclear continuum by stellar emission accounts for most of the

TABLE 4
LWP RESULTS

JD (−2,440,000)	F_{2670}[a]		Mg II $\lambda 2798$[b]	
	SIPS	GEX	SIPS	GEX
7510.085........	2.33 ± 0.19	2.24 ± 0.11	137 ± 6	123 ± 7
7514.150........	2.46 ± 0.16	2.41 ± 0.13	123 ± 6	125 ± 8
7517.994........	2.47 ± 0.16	2.43 ± 0.14	134 ± 6	132 ± 8
7522.158........	2.66 ± 0.21	2.64 ± 0.16	134 ± 6	123 ± 9
7526.168........	2.76 ± 0.29	2.73 ± 0.18	131 ± 6	119 ± 9
7530.087........	2.62 ± 0.17	2.64 ± 0.15	137 ± 6	125 ± 8
7534.072........	2.69 ± 0.15	2.68 ± 0.12	138 ± 6	141 ± 8
7538.238........	2.94 ± 0.17	2.88 ± 0.13	145 ± 6	147 ± 9
7543.265........	3.00 ± 0.21	2.93 ± 0.14	131 ± 6	129 ± 8
7546.078........	3.02 ± 0.25	3.10 ± 0.16	143 ± 6	135 ± 8
7549.898........	2.78 ± 0.16	2.73 ± 0.12	151 ± 6	137 ± 8
7553.208........	2.83 ± 0.23	2.68 ± 0.15	130 ± 6	130 ± 8
7557.207........	2.64 ± 0.15	2.53 ± 0.14	139 ± 6	135 ± 8
7561.923........	2.27 ± 0.23	2.30 ± 0.14	130 ± 6	137 ± 8
7563.249........	2.10 ± 0.25	2.01 ± 0.14	151 ± 6	150 ± 8
7565.931[c]........	2.27 ± 0.27	2.14 ± 0.17	148 ± 6	153 ± 10
7569.919........	2.23 ± 0.16	2.13 ± 0.13	148 ± 6	131 ± 8
7573.790........	1.88 ± 0.22	1.95 ± 0.15	152 ± 6	141 ± 8
7577.879........	1.90 ± 0.17	1.82 ± 0.11	136 ± 6	136 ± 7
7581.935........	1.96 ± 0.29	1.89 ± 0.15	130 ± 6	124 ± 7
7585.990........	2.08 ± 0.16	1.95 ± 0.14	143 ± 6	138 ± 9
7590.052........	2.16 ± 0.22	1.99 ± 0.12	127 ± 6	115 ± 7
7594.063........	2.22 ± 0.22	2.07 ± 0.14	118 ± 6	128 ± 7
7598.054........	2.29 ± 0.14	2.19 ± 0.13	122 ± 6	134 ± 8
7602.054........	2.36 ± 0.13	2.34 ± 0.11	124 ± 6	114 ± 6
7606.062........	2.41 ± 0.12	2.38 ± 0.14	120 ± 6	128 ± 8
7613.755........	2.73 ± 0.13	2.68 ± 0.13	134 ± 6	134 ± 8
7617.565........	2.78 ± 0.13	2.80 ± 0.15	129 ± 6	123 ± 10
7621.657........	3.25 ± 0.17	3.23 ± 0.15	146 ± 6	133 ± 8
7625.660........	3.23 ± 0.20	3.22 ± 0.16	143 ± 6	142 ± 10
7629.803........	3.17 ± 0.15	3.07 ± 0.13	128 ± 6	116 ± 8
7633.979........	3.19 ± 0.18	3.13 ± 0.13	133 ± 6	126 ± 7
7637.969........	2.99 ± 0.24	3.05 ± 0.15	133 ± 6	128 ± 10
7642.032........	3.37 ± 0.19	3.16 ± 0.16	132 ± 6	128 ± 9
7645.956........	3.11 ± 0.24	3.05 ± 0.15	128 ± 6	122 ± 8
7649.894........	3.09 ± 0.16	3.06 ± 0.13	131 ± 6	131 ± 7
7653.901........	2.93 ± 0.17	2.90 ± 0.15	140 ± 6	139 ± 10
7657.579........	2.87 ± 0.16	2.94 ± 0.14	148 ± 6	140 ± 9
7661.564........	2.73 ± 0.19	2.71 ± 0.15	138 ± 6	116 ± 8
7665.569........	2.78 ± 0.13	2.74 ± 0.12	146 ± 6	143 ± 8
7669.551........	2.61 ± 0.16	2.60 ± 0.14	146 ± 6	149 ± 10
7673.508........	2.59 ± 0.17	2.55 ± 0.14	140 ± 6	126 ± 9
7677.577........	2.43 ± 0.14	2.36 ± 0.13	151 ± 6	152 ± 9
7680.810........	2.49 ± 0.17	2.44 ± 0.13	142 ± 6	139 ± 8
7684.887........	2.28 ± 0.17	2.22 ± 0.12	152 ± 6	153 ± 8
7684.988........	2.25 ± 0.20	2.18 ± 0.15	155 ± 6	144 ± 9
7688.801........	2.13 ± 0.15	2.07 ± 0.14	152 ± 6	155 ± 8
7692.801........	2.13 ± 0.13	2.11 ± 0.14	150 ± 6	137 ± 8
7696.815........	2.14 ± 0.16	2.04 ± 0.12	143 ± 6	144 ± 8
7700.798........	2.15 ± 0.17	2.09 ± 0.13	144 ± 6	131 ± 9
7705.491........	2.24 ± 0.17	2.19 ± 0.14	145 ± 6	138 ± 10
7709.403........	2.38 ± 0.17	2.25 ± 0.11	144 ± 6	134 ± 7
7713.396........	2.50 ± 0.10	2.41 ± 0.12	143 ± 6	142 ± 8
7717.379........	2.58 ± 0.15	2.54 ± 0.15	144 ± 6	142 ± 9
7721.403........	2.48 ± 0.16	2.47 ± 0.12	146 ± 6	143 ± 7
7725.392........	2.30 ± 0.14	2.30 ± 0.13	139 ± 6	136 ± 7
7729.729........	2.00 ± 0.16	1.96 ± 0.11	142 ± 6	144 ± 6
7733.736........	1.78 ± 0.16	1.65 ± 0.10	154 ± 6	149 ± 5
7737.721........	1.62 ± 0.17	1.57 ± 0.10	148 ± 6	136 ± 7
7741.656........	1.47 ± 0.14	1.41 ± 0.10	144 ± 6	137 ± 7
7745.620........	1.49 ± 0.13	1.46 ± 0.11	141 ± 6	125 ± 6

[a] In units of 10^{-14} ergs s^{-1} cm^{-2} Å^{-1}.
[b] In units of 10^{-14} ergs s^{-1} cm^{-2}.
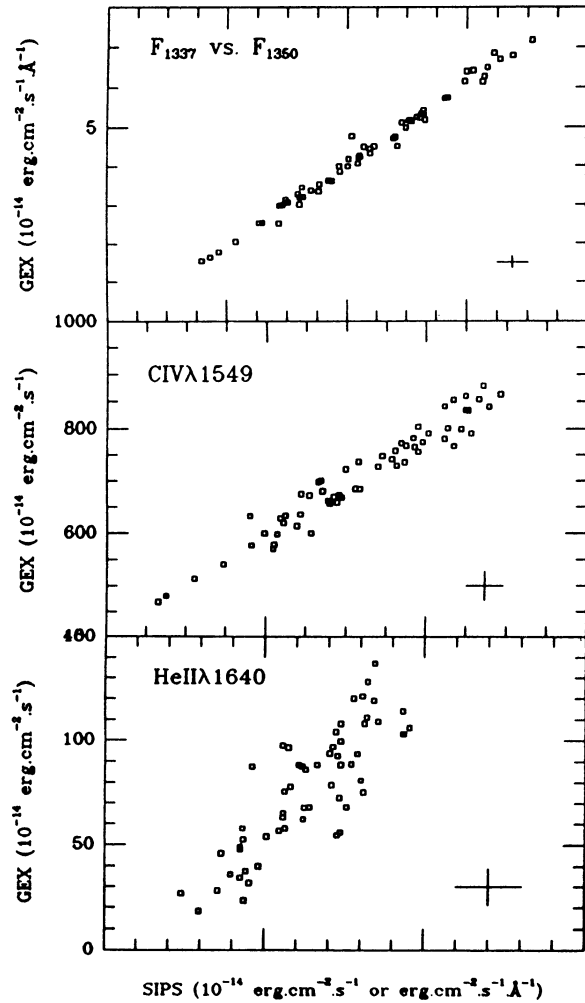[c] Vignetting correction factors: F_{2670}, 1.21; Mg II, 1.20.

FIG. 2.—Flux, as obtained with GEX, plotted as a function of the SIPS flux for the continuum near 1300 Å (*upper panel*), the C IV $\lambda 1549$ emission line (*middle panel*), and the He II $\lambda 1640$ + O III] $\lambda 1663$ blend (*lower panel*). A typical error bar is shown in the lower right-hand corner of each panel. The scale is such that the range covered is the same along the X- and the Y-axis.

reduced amplitude of the variations in the optical. Much of the diminution in variability at the longer ultraviolet wavelengths is probably due to dilution by relatively steady Fe II and Balmer continuum emission. In the SWP range, the full range of spectral index variations is $\Delta\alpha = 1.1 \pm 0.2$, with rms fluctuations $\Delta\alpha = 0.23$. Blended Fe II lines—provided that their intensity does not vary more than that of Mg II $\lambda 2798$—account for variations of ~ 0.3 in the spectral index if their contribution amounts to 10% of the 1840 Å continuum flux when it is minimum. The remaining change in α could be due to genuine spectral variations of the underlying continuum. Wamsteker *et al.* (1990), after taking into account the Fe II and Bac contribution, also find it necessary to allow for some variability (albeit small) of the optical to ultraviolet spectral index in NGC 5548, the continuum becoming systematically bluer when it brightens. A more precise estimate of the amplitude of the spectral variations will be possible when the present data are combined with the optical spectra recorded almost simultaneously (Peterson *et al.* 1990a).

All the emission-line fluxes also varied significantly. However, the amplitude of these variations differs greatly from one line to the next. The high-ionization lines N V $\lambda 1240$ and

TABLE 5

GEX versus SIPS Linear Regression

Feature	Slope	Intercept[a]	r	χ_v^2	$P(\geq \chi_v^2)$
$F_{1350/1337}$	1.048 ± 0.026	-0.17 ± 0.12	0.995	0.308	>0.999
$F_{1840/1813}$	1.010 ± 0.026	-0.00 ± 0.09	0.994	0.336	>0.999
F_{2670}	1.022 ± 0.064	-0.11 ± 0.16	0.992	0.060	>0.999
Lyα + N v	1.533 ± 0.062	-96 ± 37	0.957	0.620	0.989
C iv λ1549	0.949 ± 0.029	29 ± 30	0.975	0.455	>0.999
Mg ii λ2798	0.998 ± 0.010	-5 ± 3	0.736	0.506	>0.999
C iii] λ1909	0.868 ± 0.081	-3 ± 2	0.782	0.448	>0.999
He ii + O iii]	1.950 ± 0.102	-50 ± 14	0.827	0.979	0.520
Si iv + O iv]	1.212 ± 0.184	-3 ± 9	0.688	0.604	0.992

[a] Same units as in Tables 2–4.

TABLE 6

Variability Parameters

FEATURE	Mean Flux[a]		F_{var}		R_{max}	
	SIPS	GEX	SIPS	GEX	SIPS	GEX
$F_{1350/1337}$	4.36	4.39	0.30	0.32	4.46 ± 0.53	4.64 ± 0.29
$F_{1840/1813}$	3.31	3.33	0.26	0.27	3.45 ± 0.46	3.35 ± 0.16
F_{2670}	2.49	2.44	0.16	0.17	2.30 ± 0.25	2.29 ± 0.20
Lyα + N v	556.	760.	0.17	0.17	1.93 ± 0.09	2.14 ± 0.21
C iv λ1549	718.	708.	0.14	0.13	1.92 ± 0.11	1.87 ± 0.12
Mg ii λ2798	139.	134.	0.05	0.04	1.31 ± 0.08	1.36 ± 0.10
He ii + O iii]	64.0	77.8	0.23	0.30	3.96 ± 1.70	7.57 ± 3.02
C iii] λ1909	118.	100.	0.09	0.11	1.86 ± 0.28	2.02 ± 0.36
Si iv + O iv]	49.4	57.3	0.15	0.19	2.98 ± 1.30	3.49 ± 1.02
N v λ1240	...	89.7	...	0.49	...	56 ± 243
FES	50.6		0.08		1.37 ± 0.03	

[a] Same units as in Tables 2–4.

He ii λ1640 had variations whose amplitude was as great as or greater than that of the short-wavelength continuum, with $F_{var} \simeq 0.5$ and 0.23, respectively. Lines of intermediate ionization had lower amplitudes, with F_{var} ranging from 0.09 to 0.17 for C iv λ1549, C iii] λ1909, Lyα λ1216, and Si iv + O iv] λ1402. The lowest ionization line in our data set, Mg ii λ2798, exhibited the lowest amplitude fluctuations, with $F_{var} \simeq 0.05$. Because significant variations were found in all the emission lines, detailed structural analysis should be possible for all of them.

V. TIME SERIES ANALYSIS

The variations took the form of two large-amplitude "events," plus an additional slightly lower amplitude event near the end of the observing campaign. Here an event is defined as a statistically significant local maximum in the light

TABLE 7

Results from Cross-Correlations

Feature	Δt(Peak) (days)	Δt(Center) (days)	Amplitude	FWHM (days)
$F_{1840/1813}$	0	0	0.98	38
F_{2670}	0	0	0.97	40
FES	2	4	0.88	42
N v λ1240	4	4	0.79	34
He ii + O iii]	4	10	0.67	40
C iv λ1549	8	16	0.66	38
Lyα + N v	12	12	0.84	34
Si iv + O iv]	12	34	0.61	36
C iii] λ1909	26	32	0.56	40
Mg ii λ2798	$\simeq 34$–72		0.46	72

curve followed and preceded by a local minimum. Each individual event lasted typically $\simeq 80$–100 days, except the last one, whose duration was only about 40 days. This is in any case much larger than the interval between two consecutive observations. Hence, our temporal resolution is adequate to characterize the main ultraviolet variability of NGC 5548. Moreover, the sampling of the light curves is almost perfectly even, the mean (and error on the mean) interval between two observations being 3.99 ± 0.04 days. On top of the long-term trend are superposed a few episodes of rapid, small-amplitude variability, e.g., the dip near JD 2,447,534—most conspicuous in the light curves of Lyα, C iv, and the FES—or the "shoulder" between JD 2,447,606 and 2,447,621.

The overall resemblance of the continuum band and emission-line light curves is striking. All three major events are clearly recognizable in most light curves. There are some noticeable differences, however. For instance, during the second event, the 1350 Å continuum flux rose more rapidly than the Lyα λ1216 or C iv λ1549 emission-line flux and reached its maximum 10–15 days earlier. This suggests that the variations of the lines are delayed with respect to those of the ultraviolet continuum, as predicted by the photoionization models discussed in § I.

To quantify this delay, we computed the cross-correlation between the emission lines and the 1350 Å (and 1337 Å) continuum, as first suggested by Gaskell and Sparke (1986). Unlike previous work in this area, whose uneven sampling required either interpolation (as reviewed by Peterson 1988a) or the discrete correlation method (Edelson and Krolik 1988), our data allowed use of the conventional method. That is, at all lags τ which are integral multiples of our 4 day sampling inter-
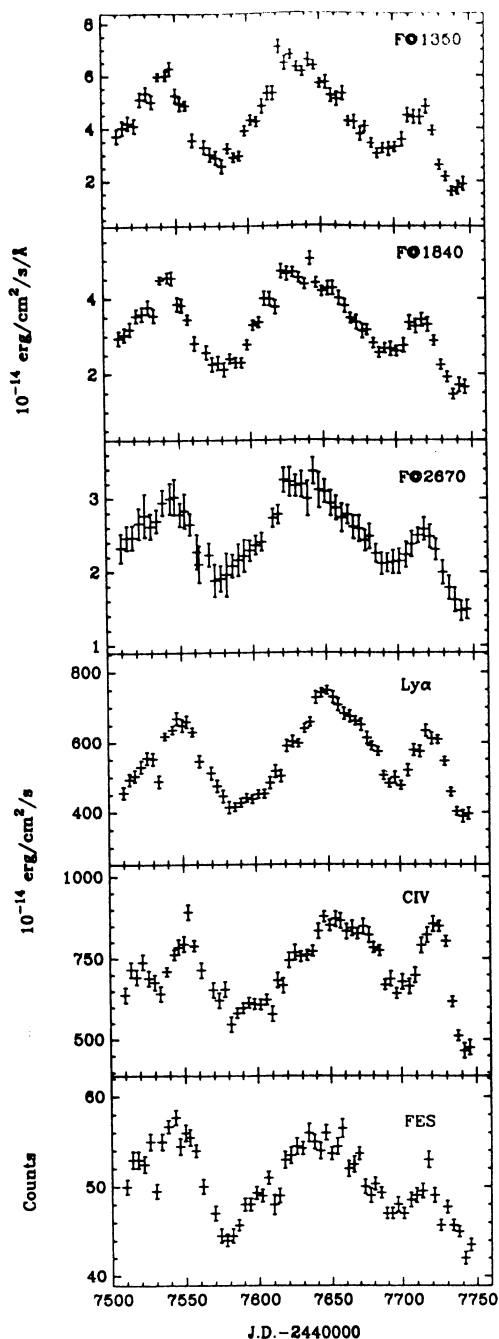
FIG. 3.—*Top to bottom*: Light curves of the continuum at 1350, 1840 and 2670 Å; the Lyα λ1216 and C IV λ1549 emission lines; and the optical light curve as measured with the FES. Units are 10^{-14} ergs cm^{-2} s^{-1} Å^{-1} for the continuum fluxes, 10^{-14} ergs cm^{-2} s^{-1} for the lines, and counts for the FES measurements. The fluxes are represented with their associated errors. Notice the large amplitude of the variations and the similarity of the light curves.

val, we computed the mean value of

$$[F_l(t_i) - \bar{F}_l][F_c(t_i - \tau) - \bar{F}_c]/(\sigma_l \sigma_c),$$

where $F_{l,c}$ is the (line, continuum) flux, and $\sigma_{l,c}$ is the standard deviation about the mean flux $\bar{F}_{l,c}$. The results are displayed in Table 7 and in Figures 5 and 6. Note that the SIPS and GEX values yield identical results. It is immediately apparent that the peak amplitude of the cross-correlation is substantial in all

cases. Only in the case of Mg II λ2798 does the correlation amplitude at the peak fall below 0.5. This fact gives very strong support to the long-held view that the ionizing continuum is the source of energy for the emission lines.

The uncertainty on the location of the maximum of these cross-correlations arises from two sources: measurement error and incomplete sampling. To assess the importance of measurement errors, we have performed a Monte Carlo simulation. Artificial light curves were generated by randomly assigning a statistically probable flux value at each epoch, that is, a value which falls within the range allowed by the measure-
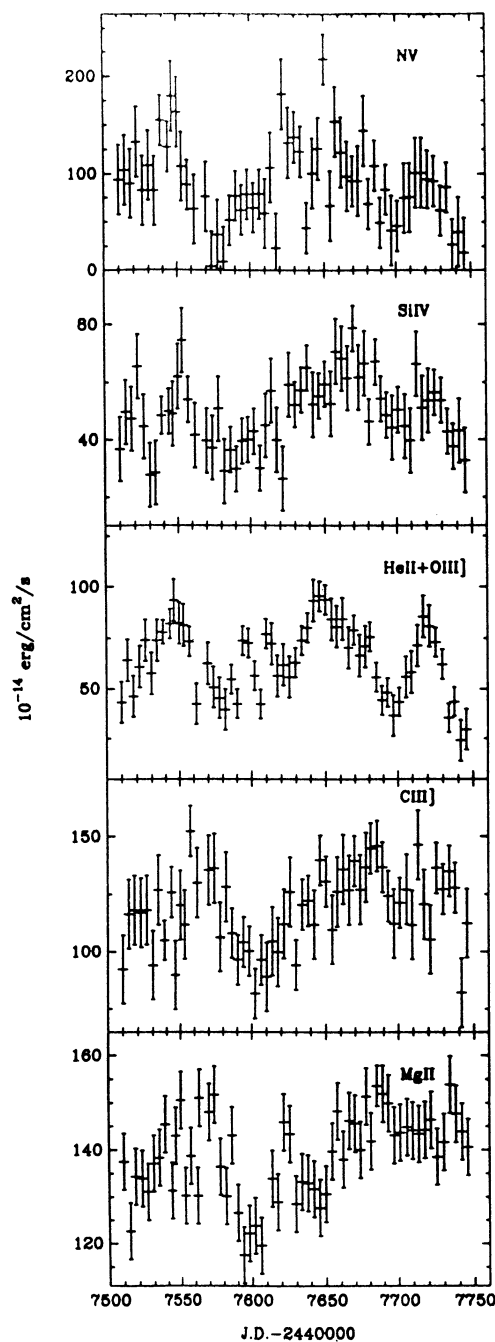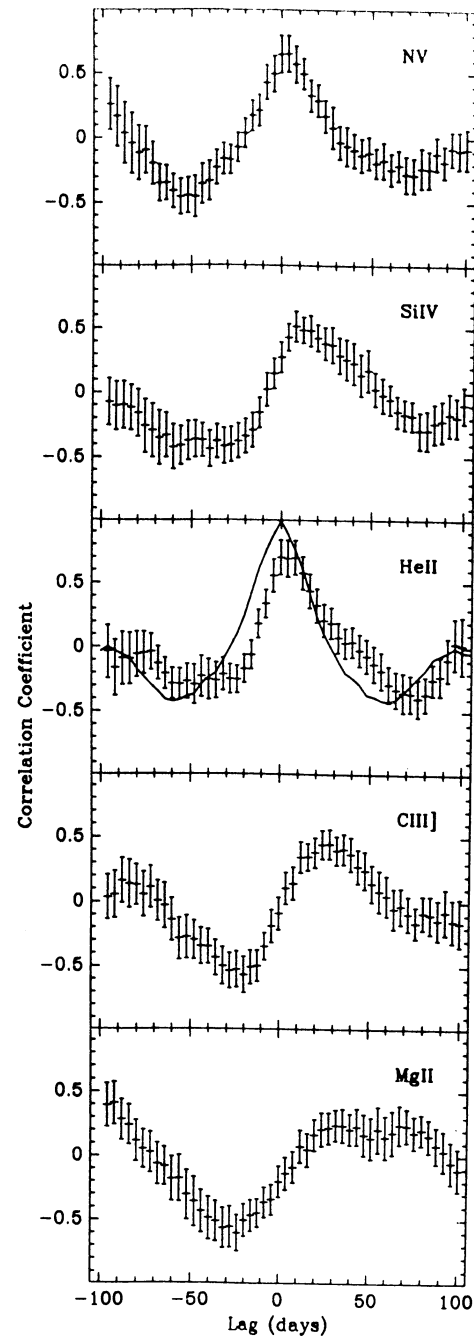

FIG. 4.—Same as Fig. 3, but for the weaker N v λ1240, Si IV + O IV] λ1402, He II λ1640 (+O III] λ1663), C III] λ1909, and Mg II λ2798 emission lines.
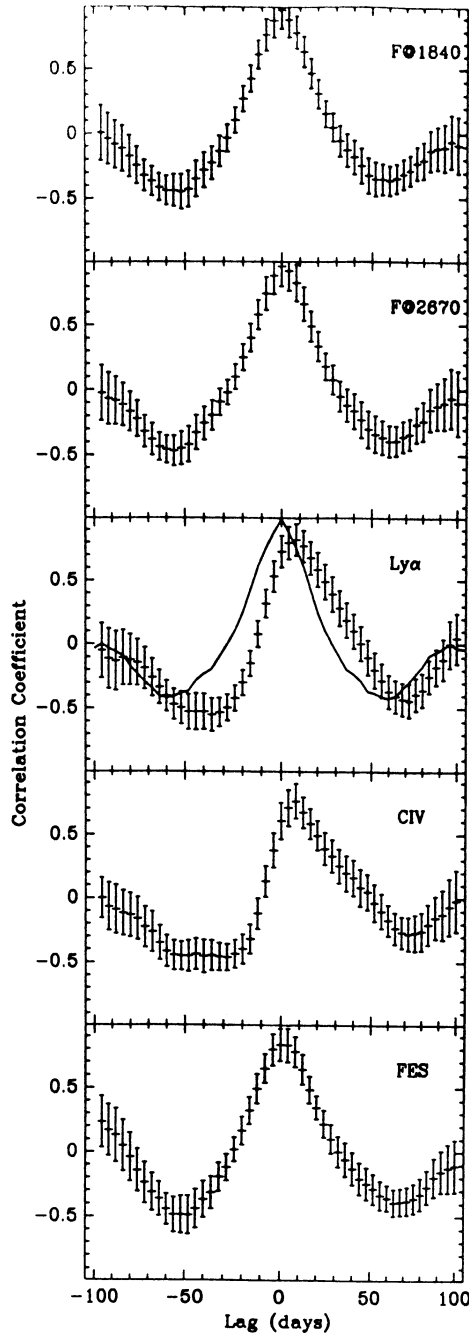
FIG. 5.—Cross-correlations (CCs) of the different emission lines and continua with the continuum flux at 1350 Å. *Top to bottom*: CC of the continuum at 1840 and at 2670 Å, of the Lyα λ1216 and C IV λ1549 emission lines, and of the FES. The points are shown with their associated errors calculated as in Edelson and Krolik (1988). For reference, the autocorrelation function of the 1350 Å continuum is shown in the panel in the middle (*fully drawn line*). Note the large value of the correlation coefficients at the peak and the very small delays of the emission lines.

analyzed. The standard deviation of these distributions gives a reliable estimate of the uncertainty on the lag due to measurement errors. This uncertainty turns out to be small: $\epsilon(\Delta t) = \pm 0.13$ and ± 0.17 days for the strong Lyα λ1216 and C IV λ1549 lines, respectively, while the weaker and noiser He II λ1640 feature yields $\epsilon(\Delta t) = \pm 1.8$ days.

Unfortunately, there is no universally accepted prescription for estimating the larger uncertainty due to incomplete sam-

FIG. 6.—Same as Fig. 5, but for the weaker N v λ1240, Si IV + O IV] λ1402, He II λ1640 (+ O III] λ1663), C III] λ1909, and Mg II λ2798 emission lines. Note the difference between the He II λ1640 line, which is well correlated at very short lags with the 1350 Å continuum, and Mg II λ2798, for which the peak of the cross-correlation is much lower and displaced toward large positive lags.

ment and its associated uncertainty. Flux values are selected in a such way that their distribution about the mean is normal. Then, each light curve is correlated with a corresponding light curve of the 1350 Å continuum obtained in the same way. The whole process is reiterated a large number of times, and the distribution of the locations of the cross-correlation peak is

pling. Several ways to obtain such errors, and to assign to them a physical meaning, are discussed by Gaskell and Peterson (1987), Edelson and Krolik (1988), and Maoz and Netzer (1989). This lack of a well-defined error estimate complicates any attempt to make quantitative use of these cross-correlation functions. An additional complication arises because the continuum autocorrelation is quite broad and smooth: consequently, the cross-correlations are, also. To illustrate this difficulty, we have listed in Table 7 the position of the peak of the cross-correlations as well as the position of their "center." By "center" we mean the average of the two lags at which the cross-correlation passes through a level 0.3 below the peak. Taken together, these two give an order-of-magnitude estimate of the characteristic delay time scale. Any difference between them indicates the degree of skewness in the cross-correlation. The FWHM of the cross-correlation function can, in principle, provide another estimate of the response time scale. If the line emission can be described as a linear convolution of the continuum light curve with a response function, the cross-correlation function is the convolution of the continuum autocorrelation function with the response function. Any difference between the FWHM of the line-continuum cross-correlation and the continuum autocorrelation would then indicate the width of the response function.

The most significant result that may be derived from Table 7 is that, apart from Mg II $\lambda2798$, all the emission lines correlate extremely well with F_{1350}, and that the characteristic delays are quite short for most of them. There is also a general tendency for the highest ionization lines to have the shortest delays. For both He II $\lambda1640$ and N V $\lambda1240$, the bulk of the cross-correlation is found in the neighborhood of 4–10 days, while for C IV $\lambda1549$ and Lyα $\lambda1216$ the range is 8–16 days. Si IV $\lambda1400$ and C III] $\lambda1909$ have cross-correlations concentrated between 12 and 34 days, while Mg II $\lambda2798$ is found from 34 to 72 days. Less significance may be attached to the fact that Lyα, N V $\lambda1240$, and Mg II $\lambda2798$ have fairly symmetric cross-correlation functions, while the cross-correlation functions for C IV $\lambda1549$, He II $\lambda1640$, and Si IV $\lambda1400$ are quite skew, with the "centers" falling at lags much larger than the peaks. In essentially all cases, the cross-correlation function (as measured by FWHM) is not much wider than the continuum autocorrelation; in other words, only rough upper limits on the widths of the response functions can be placed by this comparison.

Finally, it is worth noting that, within the uncertainties, the continuum variations occur simultaneously in all four bands, from 1350 Å to $\simeq5000$ Å.

VI. SUMMARY AND CONCLUSION

The nucleus of NGC 5548 has been observed every four days during 8 months with the *IUE* satellite. Significant variations of the emission lines and continuum flux took place. The amplitude of the variations is much larger than the measurement errors. This, together with the fact that the time scale for variability was an order of magnitude large than our sampling interval (i.e., the variations are time-resolved), allows us to draw firm and important conclusions concerning the pattern of variability of the ultraviolet (and optical) spectrum of NGC 5548.

1. The typical amplitude of the continuum variability decreases with increasing wavelength: $F_{var} = 0.30, 0.26, 0.16$, and 0.08 for $\lambda \simeq 1350, 1840, 2700$, and 5000 Å, respectively. Because all the bands are correlated at zero lag, the continuum

is systematically bluer when it is brighter. In the optical, most if not all of this effect can be attributed to dilution by stellar light. While the strong Fe II emission lines which contaminate the long-wavelength continuum and respond only very weakly to fluctuations in the continuum (Wamsteker et al. 1990) could account for much of the spectral variation in the near-ultraviolet, the changes in the spectral index observed in the SWP may, at least in part, represent a genuine property of the underlying continuum.

2. The continuum variations appear to be simultaneous in all four ultraviolet and optical bands, i.e., from $\simeq1300$ Å to 5000 Å.

3. The amplitude of variation of a given emission line seems to depend on the degree of ionization of its ion. The highest ionization lines show the strongest variations, with N V $\lambda1240$ and He II $\lambda1640$ exhibiting maximum-to-minimum flux ratios as high as those of the continuum. Intermediate-ionization lines, including Lyα $\lambda1216$, C IV $\lambda1549$, and C III] $\lambda1909$, had maximum to minimum amplitudes of $\simeq2$. Mg II $\lambda2798$, the lowest ionization line studied, exhibited the smallest amplitude fluctuations, $\simeq1.3$.

4. Apart from Mg II $\lambda2798$, the emission-line variations correlate extremely well with those of the 1350 Å continuum if allowance is made for a systematic short delay, lending qualitative support to the view that photoionization by the nuclear continuum is responsible for driving the emission lines. For Mg II the correlation is significantly weaker and the delay much longer than for other lines.

5. The delay of a given emission line seems to depend on the degree of ionization of its ion. N V $\lambda1240$ and He II $\lambda1640$ exhibit the smallest delay, the bulk of their cross-correlation being in the neighborhood of 4–10 days. The delay for the intermediate-ionization Lyα $\lambda1216$ and C IV $\lambda1549$ lines is somewhat larger, 8–16 days. The cross-correlations of Si IV + O IV] $\lambda1402$ and C III] $\lambda1909$ peak in the range 12–34 days, while that of Mg II $\lambda2798$ is concentrated at lags of from $\simeq34$ to 72 days. For comparison, a preliminary analysis of the optical data by Peterson et al. (1990a) shows that the maximum of the cross-correlation for the Hβ line occurs at a lag of $\simeq24$ days.

These results set new and strong constraints on existing and future models of the broad emission line region in active galaxies and quasars, and in particular on the geometry and the ionization structure of the BLR.

MacAlpine (Ann Arbor), Laura Maraschi (Bologna), Shingo Nakatani (UCL), Daniel Péquignot (Meudon), Mike Penston (RGO), Andy Pollock (Birmingham), Almudena Prieto (Madrid), Andy Robinson (IoA), John Michael Shull (JILA), Hartmut Schulz (Bochum), Alex Smith (University of Florida), Wayne Stein (Minneapolis), Roberto Terlevich (RGO), Megg Urry (STScI), Martin Ward (IoA), Mark Whittle (Charlottesville), and Bev and Derek Wills (Austin).

REFERENCES

Andrillat, Y., and Souffrin, S. 1968, *Ap. Letters*, **1**, 111.
Avni, Y. 1976, *Ap. J.*, **210**, 642.
Barr, P., Willis, A. J., and Wilson, R. 1983, *M.N.R.A.S.*, **203**, 201.
Barylak, M., Wasatonic, R., and Imhoff, C. 1984, *ESA IUE Newsletter*, **20**, 201.
Blandford, R. D., and McKee, C. F. 1982, *Ap. J.*, **255**, 419.
Boggess, A., *et al.* 1978a, *Nature*, **275**, 372.
Boggess, A., *et al.* 1978b, *Nature*, **275**, 377.
Bohlin, R. 1988, *NASA IUE Newsletter*, **34**, 10.
Bohlin, R. C., Holm, A. V., Savage, B. D., Snijders, M. A. J., and Sparks, W. M. 1980, *Astr. Ap.*, **85**, 1.
Branduardi-Raymont, G. 1988, in *IAU Symposium 134, Active Galactic Nuclei*, ed. D. E. Osterbrock and J. S. Miller (Dordrecht: Kluwer), p. 177.
Capriotti, E. R., Foltz, C. B., and Peterson, B. M. 1982, *Ap. J.*, **261**, 35.
Cassatella, A., Barbero, J., and Benvenuti, P. 1985, *Astr. Ap.*, **144**, 335 (CBB).
Cherepashchuk, A. M., and Lyutyi, V. M. 1973, *Ap. Letters*, **13**, 165.
Clavel, J., *et al.* 1987, *Ap. J.*, **321**, 251.
Clavel, J., Wamsteker, W., and Glass, I. S. 1989, *Ap. J.*, **337**, 236.
Davidson, K., and Netzer, H. 1979, *Rev. Mod. Phys.*, **51**, 715.
Dibai, E. A., and Pronik, V. I. 1967, *Astr. Zh.*, **44**, 952.
Edelson, R. A., and Krolik, J. H. 1988, *Ap. J.*, **333**, 646.
Edelson, R. A., and Malkan, M. A. 1986, *Ap. J.*, **308**, 59.
Faelker, J., Gordon, F., and Sandford, M. C. W. 1987, in *Exploring the Universe with the IUE Satellite*, ed. Y. Kondo *et al.* (Dordrecht: Reidel), p. 21.
Fitch, W., Pacholczyk, A. G., and Weymann, R. J. 1967, *Ap. J. (Letters)*, **150**, L67.
Gaskell, C. M., and Peterson, B. M. 1987, *Ap. J. Suppl.*, **65**, 1.
Gaskell, C. M., and Sparke, L. S. 1986, *Ap. J.*, **305**, 175.
Gregory, S., Ptak, R., and Stoner, R. 1982, *Ap. J.*, **261**, 30.
Harris, A. W., and Sonneborn, G. 1987, in *Exploring the Universe with the IUE Satellite*, ed. Y. Kondo *et al.* (Dordrecht: Reidel), p. 729.
Holm, A. V., and Crabb, W. G. 1979, *NASA IUE Newsletter*, **7**, 40.

Holm, A. V., and Rice, G. 1981, *NASA IUE Newsletter*, **15**, 74.
Kaastra, J. S., and Barr, P. 1989, *Astr. Ap.*, **226**, 59.
Koratkar, A. P., and Gaskell, C. M. 1989, *Ap. J.*, **345**, 637.
Maoz, D., and Netzer, H. 1989, *M.N.R.A.S.*, **236**, 21.
Maoz, D., *et al.* 1990, *Ap. J.*, **351**, 75.
Munoz-Peiro, J. R. 1985, *NASA IUE Newsletter*, **27**, 27.
Netzer, H., *et al.* 1990, *Ap. J.*, **353**, 108.
Netzer, H., and Wills, B. J. 1983, *Ap. J.*, **275**, 445.
Peterson, B. M. 1988a, *Pub. A.S.P.*, **100**, 18.
———. 1988b, *IAU Circ.*, No. 4664.
Peterson, B. M., Korista, K. T., and Wagner, R. M. 1989, *A.J.*, **98**, 500.
Peterson, B. M., *et al.* 1990a, in *Proc. Conf. on Variability of Active Galactic Nuclei* (Atlanta), ed. H. R. Miller and P. J. Wiita (Cambridge: Cambridge University Press).
Peterson, B. M., Reichert, G. A., Korista, K. T., and Wagner, R. M. 1990b, *Ap. J.*, **352**, 68.
Reichert, G. A., and Kriss, G. 1990, in preparation.
Rosenblatt, E. I., and Malkan, M. A. 1990, *Ap. J.*, **350**, 132.
Sonneborn, G., Oliversen, N. A., Imhoff, C. L., Pitts, R. E., and Holm, A. V. 1987, *NASA IUE Newsletter*, **32**, 6.
Turner, T. J., and Pounds, K. 1989, *M.N.R.A.S.*, **240**, 833.
Turnrose, B. E., and Thompson, R. W. 1984, *IUE Image Processing Information Manual, Version 2.0*, CSC/TM-84/6058.
Ulrich, M. H., *et al.* 1984, *M.N.R.A.S.*, **206**, 221.
Urry, M., and Reichert, G. 1988, *NASA IUE Newsletter*, **34**, 95.
Wamsteker, W., *et al.* 1990, *Ap. J.*, **354**, 446.
Wills, B. J., Netzer, H., and Wills, D. 1985, *Ap. J.*, **248**, 472.
Wilson, A. S., and Ulvestad, J. S. 1982, *Ap. J.*, **260**, 56.
Wilson, A. S., Wu, X., Baldwin, J. A., and Balick, B. 1989, *Ap. J.*, **339**, 729.
York, D. 1966, *Canadian J. Phys.*, **44**, 1079.